5-1992

A Three-Dimensional Environmental Fluid Dynamics Computer Code : Theoretical and computational aspects

John M. Hamrick
Virginia Institute of Marine Science

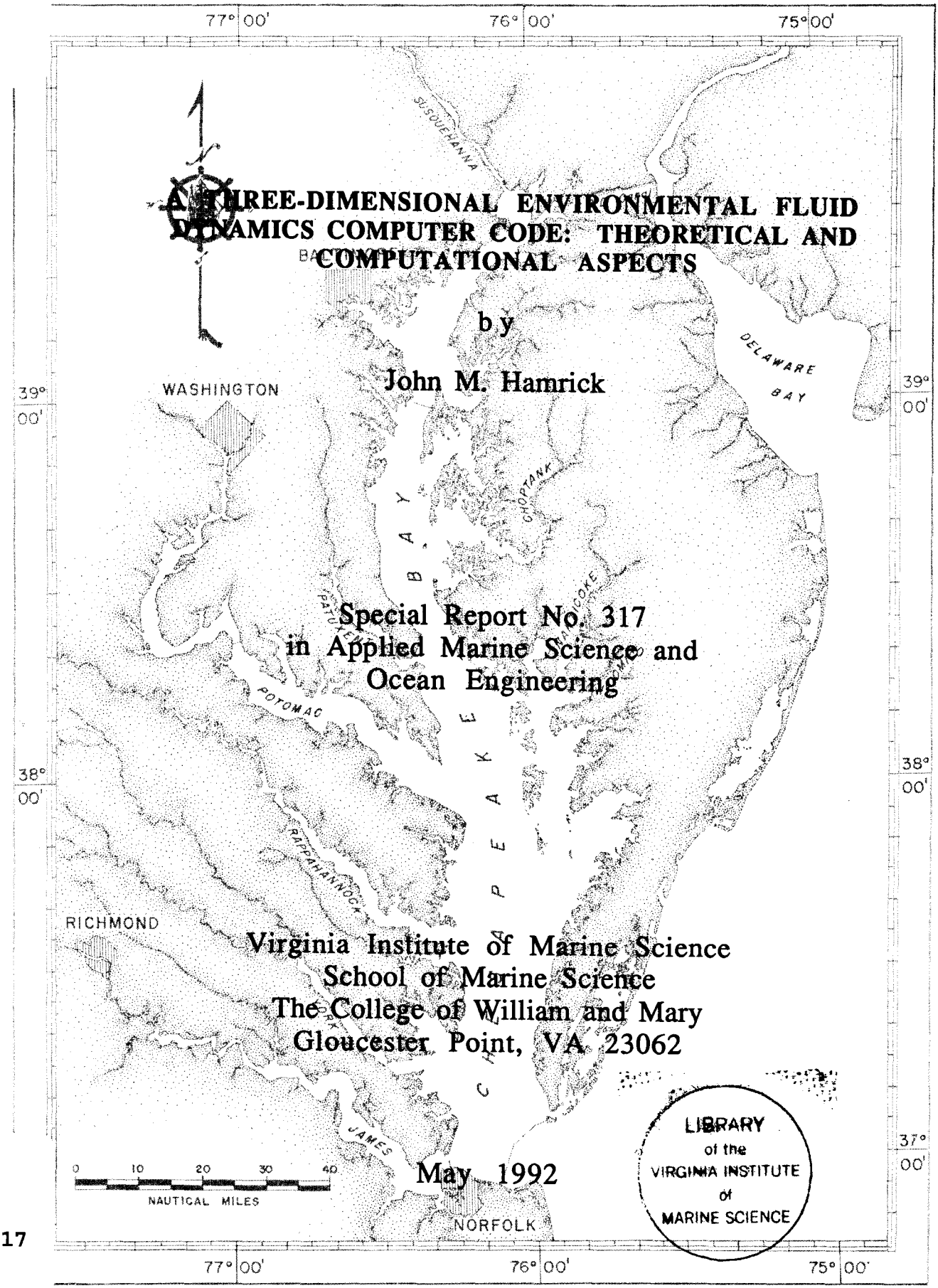

A THREE-DIMENSIONAL ENVIRONMENTAL FLUID DYNAMICS COMPUTER CODE: THEORETICAL AND COMPUTATIONAL ASPECTS

by

John M. Hamrick

Special Report No. 317
in Applied Marine Science and
Ocean Engineering

Virginia Institute of Marine Science
School of Marine Science
The College of William and Mary
Gloucester Point, VA 23062

May 1992

A THREE-DIMENSIONAL ENVIRONMENTAL FLUID DYNAMICS COMPUTER CODE: THEORETICAL AND COMPUTATIONAL ASPECTS

b y

John M. Hamrick

Special Report No. 317
in Applied Marine Science and
Ocean Engineering

Virginia Institute of Marine Science
School of Marine Science
The College of William and Mary
Gloucester Point, VA 23062

May 1992

ABSTRACT

This report describes and documents the theoretical and computational aspects of a three-dimensional computer code for environmental fluid flows. The code solves the three-dimensional primitive variable vertically hydrostatic equations of motion for turbulent flow in a coordinate system which is curvilinear and orthogonal in the horizontal plane and stretched to follow bottom topography and free surface displacement in the vertical direction which is aligned with the gravitational vector. A second moment turbulence closure scheme relates turbulent viscosity and diffusivity to the turbulence intensity and a turbulence length scale. Transport equations for the turbulence intensity and length scale as well as transport equations for salinity, temperature, suspended sediment and a dye tracer are also solved. An equation of state relates density to pressure, salinity, temperature and suspended sediment concentration.

The computational scheme utilizes an external-internal mode splitting to solve the horizontal momentum equations and the continuity equation on a staggered grid. The external mode, associated with barotropic long wave motion, is solved using a semi-implicit three time level scheme with a periodic two time level correction. A multi-color successive over relaxation scheme is used to solve the resulting system of equations for the free surface displacement. The internal mode, associated with vertical shear of the horizontal velocity components is solved using a fractional step scheme combining an implicit step for the vertical shear terms, with an explicit step for all other terms. The transport equations for the turbulence intensity, turbulence length scale, salinity, temperature, suspended sediment and dye tracer are also solved using a fractional step scheme with implicit vertical diffusion and explicit advection and horizontal diffusion. A number of alternate advection schemes are implemented in the code.

ACKNOWLEDGEMENT

The work described in this report was funded by the Commonwealth of Virginia under the Three-Dimensional Model Research Initiative at the Virginia Institute of Marine Science, College of William and Mary. Many members of the VIMS faculty and staff provided advice, encouragement and support during the development of the environmental fluid dynamics computer code described in this report. Dr. Albert Y. Kuo is thanked for his continued technical advice and encouragement. The administrative support of Drs. Robert J. Byrne and Bruce J. Neilson is gratefully acknowledged. Mr. Gamble M. Sisson, Ms. Sarah Rennie, and Mr. John N. Posenau are thanked for their support in data analysis, graphics programming and computer systems management.

CONTENTS

List of Figures

1. INTRODUCTION

The ability to predict the transport and mixing of materials discharged into the hydrosphere and atmosphere is an essential element in environmental management. The field of environmental fluid dynamics has emerged in response to the need to understand and predict environmental fluid flows and the associated transport and mixing for dissolved and suspended materials in these flows. A large range of space and time scales characterize transport and mixing in the hydrologic and atmospheric environments. For example, local mixing associated with the discharge of a buoyant waste fluid into an ambient environmental flow can be described in terms of the three dimensional dynamics of buoyant turbulent jets and plumes (Fischer *et al*, 1979). Outside of this region of local or initial mixing, the further mixing and transport of discharged material is governed by the dynamics of the ambient environmental flow.

A large class of incompressible ambient environmental flows are characterized by horizontal length scales which are orders of magnitude greater than their vertical length scales or length scales in the direction aligned with the gravitational vector. Such flows are essentially hydrostatic in the vertical and of the boundary layer type. Example flows in the hydrosphere range from rivers and lakes through estuaries and coastal seas to ocean basins. Similarly in the atmosphere, mesoscale through global scale circulation can be described by equations of motion simplified by the hydrostatic and boundary layer approximations. This class of natural environmental flows is also characterized by complex boundaries and topography and a host of nonlinear processes. The realistic simulation of these complex flows necessitates the numerical solution of the equations of motions and transport equations describing the transport and mixing of dissolved and suspended materials.

The development of numerical or computational techniques appropriate for the solution of the incompressible, vertically

hydrostatic equations of motion occurred largely in the field of numerical weather prediction. The monograph by Haltiner and Williams (1980) and the volume edited by Chang (1977) provide excellent descriptions of the techniques developed through the late 1970's. These techniques provided the basis for the development of numerical ocean circulation models such as those of Bryan (1969) and Semtner (1974). The growing concern for environmental problems in lakes, estuaries and the coastal ocean lead to further development in numerical techniques and models appropriate for these flow environments as typified by the work of Simons (1974), Liu and Leendertse (1975), and Blumberg and Mellor (1987). Continuing developments in estuarine and oceanic numerical modeling are presented in the recent volumes edited by Heaps (1987) and Nihoul and Jamart (1987), while the text by Pielke (1984) presents parallel developments in the modeling mesoscale atmospheric flows.

The purpose of the work presented herein is to formulate a numerical solution scheme for incompressible, vertically hydrostatic environmental flows in the hydrosphere and atmosphere, and to implement computationally that scheme in a computer code appropriate for the range of computing platforms from personal to super computers. In formulating the numerical solution scheme, the goal is not to reinvent the wheel, but to build upon the large foundation of previous work briefly referenced in the preceding paragraph, and extend it when appropriate to achieve improvements in accuracy, stability and performance. The first version of the code and certain terminology in this report is focused toward hydrospheric flows in estuaries and the coastal ocean, as well as lakes, reservoirs and rivers. However, care has be taken to make the solution scheme and code readily applicable to analeastic hydrostatic atmospheric flows by a simple substitution of an appropriate equation of state. The remainder of the paper is organized as follows. The governing equations of motion and transport equations are formulated in Section 2. The overall numerical scheme for the equations of motion based on internal, external mode splitting is

presented in Section 3. Section 4 contains the formulation of the numerical scheme for the external or long surface gravity wave mode and an analysis of its stability and propagation characteristics. The internal, vertical shear or boundary layer mode numerical scheme is presented in Section 5. The numerical schemes for the transport equations are presented in Section 6. The computational aspects of the various numerical schemes are also discussed in Sections 4, 5, and 6. Section 7 describes the computational implementation of the numerical schemes in Environmental Fluid Dynamics Computer Code (EFDC), and outlines a strategy for the code's application to environmental fluid flow simulation and its complementary use as a research tool. Lastly, Section 8 summarizes the important features of the numerical scheme and the environmental fluid dynamics computer code.

2. FORMULATION OF THE GOVERNING EQUATIONS

The formulation of the governing equations for ambient environmental flows characterized by horizontal length scales which are orders of magnitude greater than their vertical length scales begins with the vertically hydrostatic, boundary layer form of the turbulent equations of motion for an incompressible, variable density fluid. To accommodate realistic horizontal boundaries, it is convenient to formulate the equations such that the horizontal coordinates, x and y, are curvilinear and orthogonal. To provide uniform resolution in the vertical direction, aligned with the gravitational vector and bounded by bottom topography and a free surface permitting long wave motion, a time variable mapping or stretching transformation is desirable. The mapping or stretching is given by:

$$z = (z^* + h)/(\zeta + h) \tag{1}$$

where * denotes the original physical vertical coordinates and -h and ζ are the physical vertical coordinates of the bottom topography and the free surface respectively, Figure 1. Details of the transformation may be found in Vinokur (1974), Blumberg and Mellor (1987) or Hamrick (1986). Transforming the vertically hydrostatic boundary layer form of the turbulent equations of motion and utilizing the Boussinesq approximation for variable density results in the momentum and continuity equations and the transport equations for salinity and temperature in the following form:

$$\partial_t(mHu)+\partial_x(m_yHuu)+\partial_y(m_xHvu)+\partial_z(mwu)-(mf+v\partial_x m_y-u\partial_y m_x)Hv$$
$$=-m_yH\partial_x(g\zeta+p)-m_y(\partial_x h-z\partial_x H)\partial_z p+\partial_z(mH^{-1}A_v\partial_z u)+Q_u \qquad (2)$$

$$\partial_t(mHv)+\partial_x(m_yHuv)+\partial_y(m_xHvv)+\partial_z(mwv)+(mf+v\partial_x m_y-u\partial_y m_x)Hu$$
$$=-m_xH\partial_y(g\zeta+p)-m_x(\partial_y h-z\partial_y H)\partial_z p+\partial_z(mH^{-1}A_v\partial_z v)+Q_v \qquad (3)$$

$$\partial_z p=-gH(\rho-\rho_o)\rho_o^{-1}=-gHb \qquad (4)$$

$$\partial_t(m\zeta)+\partial_x(m_yHu)+\partial_y(m_xHv)+\partial_z(mw)=0 \qquad (5)$$

$$\partial_t(m\zeta)+\partial_x(m_yH\int_0^1 udz)+\partial_y(m_xH\int_0^1 vdz)=0 \qquad (6)$$

$$\rho=\rho(p,S,T) \qquad (7)$$

$$\partial_t(mHS)+\partial_x(m_yHuS)+\partial_y(m_xHvS)+\partial_z(mwS)=\partial_z(mH^{-1}A_b\partial_z S)+Q_S \qquad (8)$$

$$\partial_t(mHT)+\partial_x(m_yHuT)+\partial_y(m_xHvT)+\partial_z(mwT)=\partial_z(mH^{-1}A_b\partial_z T)+Q_T. \qquad (9)$$

In these equations, u and v are the horizontal velocity components in the curvilinear, orthogonal coordinates x and y, m_x and m_y are the square roots of the diagonal components of the metric tensor, $m = m_x m_y$ is the Jacobian or square root of the metric tensor determinant. The vertical velocity, with physical units, in the

stretched, dimensionless vertical coordinate z is w, and is related to the physical vertical velocity w* by:

$$w = w^* - z(\partial_t \zeta + u m_x^{-1} \partial_x \zeta + v m_y^{-1} \partial_y \zeta) + (1 - z)(u m_x^{-1} \partial_x h + v m_y^{-1} \partial_y h) \quad (10)$$

The total depth, H= h + ζ, is the sum of the depth below and the free surface displacement relative to the undisturbed physical vertical coordinate origin, z* = 0. The pressure p is the physical pressure in excess of the reference density hydrostatic pressure, $\rho_o g H(1 - z)$, divided by the reference density, ρ_o. In the momentum equations (2, 3) f is the Coriolis parameter, A_v is the vertical turbulent or eddy viscosity, and Q_u and Q_v are momentum source-sink terms which will be later modeled as subgrid scale horizontal diffusion. The density, ρ, is in general a function of temperature, T, and salinity or water vapor, S, in hydrospheric and atmospheric flows respectively and can be a weak function of pressure, consistent with the incompressible continuity equation under the anelastic approximation (Mellor, 1991, Clark and Hall, 1991). The buoyancy, b, is defined in equation (4) as the normalized deviation of density from the reference value. The continuity equation (5) has been integrated with respect to z over the interval (0,1) to produce the depth integrated continuity equation (6) using the vertical boundary conditions, w = 0, at z = (0,1), which follows from the kinematic conditions and equation (10). In the transport equations for salinity and temperature (8,9) the source and sink terms, Q_S and Q_T include subgrid scale horizontal diffusion and thermal sources and sinks, while A_b is the vertical turbulent diffusivity. It is noted that constraining the free surface displacement to be time independent and spatially constant yields the equivalent of the rigid lid ocean circulation equations employed by Smetner (1974) and equations similar to the terrain following equations used by Clark (1977) to model mesoscale atmospheric flow.

The system of eight equations (2-9) provides a closed system for the variables u, v, w, p, ζ, ρ, S, and T, provided that the vertical

turbulent viscosity and diffusivity and the source and sink terms are specified. To provide the vertical turbulent viscosity and diffusivity, the second moment turbulence closure model developed by Mellor and Yamada (1982) and modified by Galperin *et al* (1988) will be used. The model relates the vertical turbulent viscosity and diffusivity to the turbulent intensity, qq, a turbulent length scale, *l*, and a Richardson number Rq by:

$$A_v = \phi_v q l = 0.4(1+36R_q)^{-1}(1+6R_q)^{-1}(1+8R_q)ql \tag{11}$$

$$A_b = \phi_b q l = 0.5(1+36R_q)^{-1} ql \tag{12}$$

$$R_q = \frac{gH\partial_z b}{q^2}\frac{l^2}{H^2}. \tag{13}$$

where the so-called stability functions ϕ_v and ϕ_b account for reduced and enhanced vertical mixing or transport in stable and unstable vertically density stratified environments, respectively. The turbulence intensity and the turbulence length scale are determined by a pair of transport equations:

$$\partial_t(mHq^2) + \partial_x(m_y Huq^2) + \partial_y(m_x Hvq^2) + \partial_z(mwq^2) = \partial_z(mH^{-1}A_q\partial_z q^2) + Q_q$$
$$+2mH^{-1}A_v\left((\partial_z u)^2 + (\partial_z v)^2\right) + 2mgA_b\partial_z b - 2mH(B_1 l)^{-1}q^3 \tag{13}$$

$$\partial_t(mHq^2 l) + \partial_x(m_y Huq^2 l) + \partial_y(m_x Hvq^2 l) + \partial_z(mwq^2 l) = \partial_z(mH^{-1}A_q\partial_z q^2 l) + Q_l$$
$$+mH^{-1}E_1 l A_v\left((\partial_z u)^2 + (\partial_z v)^2\right) + mgE_1E_3 l A_b\partial_z b - mHB_1^{-1}q^3\left(1+E_2(\kappa L)^{-2}l^2\right) \tag{14}$$

$$L^{-1} = H^{-1}\left(z^{-1} + (1-z)^{-1}\right), \tag{15}$$

where B1, E1, E2, and E3 are empirical constants and Qq and Q*l* are additional source-sink term such as subgrid scale horizontal diffusion. The vertical diffusivity, Aq, is in general taken equal to the vertical turbulent viscosity, Av.

3. NUMERICAL SOLUTION TECHNIQUES FOR THE EQUATIONS OF MOTION

The equations of motion (2-6) will be solved in a region subdivided into six faced cells. The projection of the vertical cell boundaries to a horizontal plane forms a curvilinear, orthogonal grid in the orthogonal coordinate system (x,y). In a vertical (x,z) or (y,z) plane, the cells bounded by the same constant z surfaces will be referred to as cell layers or layers. The equations will be solved using a combination of finite volume and finite difference techniques, with the variable locations shown in Figure 2. The staggered grid location of variables is often referred to as the C grid (Arakawa and Lamb, 1977) or the MAC grid (Peyret and Taylor, 1983). To proceed, it is convenient to modify equations (2,3) by eliminating the vertical pressure gradients using equation (4). After some manipulation, the horizontal momentum equations become:

$$\partial_t(mHu)+\partial_x(m_yHuu)+\partial_y(m_xHvu)+\partial_z(mwu)-(mf+v\partial_x m_y-u\partial_y m_x)Hv$$
$$=-m_yH\partial_x p-m_yHg\partial_x\zeta+m_yHgb\partial_x h-m_yHgbz\partial_x H+\partial_z(mH^{-1}A_v\partial_z u)+Q_u \qquad (16)$$

$$\partial_t(mHv)+\partial_x(m_yHuv)+\partial_y(m_xHvv)+\partial_z(mwv)+(mf+v\partial_x m_y-u\partial_y m_x)Hu$$
$$=-m_xH\partial_y p-m_xHg\partial_y\zeta+m_xHgb\partial_y h-m_xHgbz\partial_y H+\partial_z(mH^{-1}A_v\partial_z v)+Q_v \qquad (17)$$

The vertical discretization of Equations (16, 17) is considered first. The equations are integrated with respect to z over a cell layer assuming that variables defined vertically at the cell or layer centers are constant and that variables defined vertically at the cell layer interfaces or boundaries vary linearly over the cell, to give:

$$\partial_t(mH\Delta_k u_k)+\partial_x(m_yH\Delta_k u_k u_k)+\partial_y(m_xH\Delta_k v_k u_k)+(mwu)_k-(mwu)_{k-1}$$
$$-(mf+v_k\partial_x m_y-u_k\partial_y m_x)\Delta_k Hv_k=-0.5m_yH\Delta_k\partial_x(p_k+p_{k-1})-m_yH\Delta_k g\partial_x\zeta$$
$$+m_yH\Delta_k gb_k\partial_x h-0.5m_yH\Delta_k gb_k(z_k+z_{k-1})\partial_x H+m(\tau_{xx})_k-m(\tau_{xx})_{k-1}+(\Delta Q_u)_k \qquad (18)$$

$$\partial_t(mH\Delta_k v_k)_k + \partial_x(m_y H\Delta_k u_k v_k) + \partial_y(m_x H\Delta_k v_k v_k) + (mwv)_k - (mwv)_{k-1}$$
$$+(mf + v_k\partial_x m_y - u_k\partial_y m_x)\Delta_k H u_k = -0.5m_x H\Delta_k\partial_y(p_k + p_{k-1}) - m_x H\Delta_k g\partial_y\zeta$$
$$+m_x H\Delta_k g b_k\partial_y h - 0.5m_x H\Delta_k g b_k(z_k + z_{k-1})\partial_y H + m(\tau_{yz})_k - m(\tau_{yz})_{k-1} + (\Delta Q_v)_k \qquad (19)$$

where Δk is the vertical cell or layer thickness and the turbulent shear stresses at the cell layer interfaces are defined by:

$$(\tau_{xz})_k = 2H^{-1}(A_v)_k(\Delta_{k+1} + \Delta_k)^{-1}(u_{k+1} - u_k) \qquad (20)$$

$$(\tau_{yz})_k = 2H^{-1}(A_v)_k(\Delta_{k+1} + \Delta_k)^{-1}(v_{k+1} - v_k) \qquad (21)$$

If there are K cells in the z direction, the hydrostatic equation can be integrated from a cell layer interface to the surface to give:

$$p_k = gH\left(\sum_{j=k}^{K}\Delta_j b_j - \Delta_k b_k\right) + p_s \qquad (22)$$

where ps is the physical pressure at the free surface or under the rigid lid divided by the reference density. The continuity equation (5) is also integrated with respect to z over a cell or layer to give:

$$\partial_t(m\Delta_k\zeta) + \partial_x(m_y H\Delta_k u_k) + \partial_y(m_x H\Delta_k v_k) + m(w_k - w_{k-1}) = 0 \qquad (23)$$

The numerical solution of the vertically discrete momentum equations (18,19) now proceeds by splitting the external depth integrated mode associated with external long surface gravity waves from the internal mode associated with vertical current structure.

The external mode equations are obtained by summing equations (18,19) over K cells or layers in the vertical utilizing equation (22),

and are given by:

$$\partial_t(mH\bar{u})+\sum_{k=1}^{K}\left(\partial_x(m_yH\Delta_k u_k u_k)+\partial_y(m_xH\Delta_k v_k u_k)-H(mf+v_k\partial_x m_y-u_k\partial_y m_x)\Delta_k v_k\right)$$
$$=-m_yHg\partial_x\zeta-m_yH\partial_x p_s+m_yHg\bar{b}\,\partial_x h-m_yHg\left(\sum_{k=1}^{K}\left(\Delta_k\beta_k+0.5\Delta_k(z_k+z_{k-1})b_k\right)\right)\partial_x H$$
$$-0.5m_yH^2\partial_x\left(\sum_{k=1}^{K}\Delta_k\beta_k\right)+m(\tau_{xx})_K-m(\tau_{xx})_0+\overline{Q_u} \tag{24}$$

$$\partial_t(mH\bar{v})+\sum_{k=1}^{K}\left(\partial_x(m_yH\Delta_k u_k v_k)+\partial_y(m_xH\Delta_k v_k v_k)+H(mf+v_k\partial_x m_y-u_k\partial_y m_x)\Delta_k u_k\right)$$
$$=-m_xHg\partial_y\zeta-m_xH\partial_y p_s+m_xHg\bar{b}\,\partial_y h-m_xHg\left(\sum_{k=1}^{K}\left(\Delta_k\beta_k+0.5\Delta_k(z_k+z_{k-1})b_k\right)\right)\partial_y H$$
$$-0.5m_xH^2\partial_y\left(\sum_{k=1}^{K}\Delta_k\beta_k\right)+m(\tau_{yz})_K-m(\tau_{yz})_0+\overline{Q_v} \tag{25}$$

$$\partial_t(m\zeta)+\partial_x(m_yH\bar{u})+\partial_y(m_xH\bar{v})=0 \tag{26}$$

$$\beta_k=\sum_{j=k}^{K}\Delta_j b_j-0.5\Delta_k b_k \tag{27}$$

where the over bar indicates an average over the depth. The depth integrated continuity equation (26) follows from equation (6) and provides the continuity constraint for the external mode. Consistent with the form of equation (26), the external mode variables will be chosen to be the free surface displacement, ζ, and the volumetric transports myHu and mxHv. Details of the solution of the external mode equations (24-26) are presented in Section 4.

A number of formulations are possible for the internal mode equations. Equations (18,19) have K degrees of freedom for each of the horizontal velocity components. However, the summation of these equations over K cells or layers in the vertical to form the external mode equations (24,25) effectively removes a degree of

freedom since the constraints:

$$\sum_{k=1}^{K} \Delta_k u_k = \bar{u} \tag{28}$$

$$\sum_{k=1}^{K} \Delta_k v_k = \bar{v} \tag{29}$$

must be satisfied. One approach to the internal mode is to solve equations (18,19) using the free surface slopes, or the surface pressure gradients in the rigid lid case, from the external solution and distribute the error such that equations (28,29) are satisfied. A second approach is to form equations for the deviations of the velocity components from their vertical means by subtracting the external equations (24,25) from the layer integrated equations (18,19). However, it will still be necessary to satisfy the constraints (28,29). The approach proposed herein is to reduce the systems of K layer averaged equations (18,19) to systems of K-1 equations and use equations (28,29) to provide the Kth equation consistent with the actual degrees of freedom.

The internal mode equations are formed by dividing equations (18,19) by the cell layer thickness, Δk, subtracting the equations for cell layer k from the equations for cell layer k+1, and then dividing the results by the average thickness of the two cell layers to give:

$$\begin{aligned}
&\partial_t\left(mH\Delta^{-1}_{k+1,k}(u_{k+1}-u_k)\right)+\partial_x\left(m_yH\Delta^{-1}_{k+1,k}(u_{k+1}u_{k+1}-u_ku_k)\right)+\partial_y\left(m_xH\Delta^{-1}_{k+1,k}(v_{k+1}u_{k+1}-v_ku_k)\right)\\
&+m\Delta^{-1}_{k+1,k}\left(\Delta^{-1}_{k+1}\left((wu)_{k+1}-(wu)_k\right)-\Delta^{-1}_{k}\left((wu)_k-(wu)_{k-1}\right)\right)\\
&-\Delta^{-1}_{k+1,k}\left((mf+v_{k+1}\partial_xm_y-u_{k+1}\partial_ym_x)Hv_{k+1}-(mf+v_k\partial_xm_y-u_k\partial_ym_x)Hv_k\right)\\
&=m_yH\Delta^{-1}_{k+1,k}g(b_{k+1}-b_k)(\partial_xh-z_k\partial_xH)-0.5m_yH^2\Delta^{-1}_{k+1,k}g(\Delta_{k+1}\partial_xb_{k+1}+\Delta_k\partial_xb_k)\\
&+m\Delta^{-1}_{k+1,k}\left(\Delta^{-1}_{k+1}\left((\tau_{xx})_{k+1}-(\tau_{xx})_k\right)-\Delta^{-1}_{k}\left((\tau_{xx})_k-(\tau_{xx})_{k-1}\right)\right)+\Delta^{-1}_{k+1,k}\left((Q_u)_{k+1}-(Q_u)_k\right)
\end{aligned} \tag{30}$$

$$\partial_t\left(mH\Delta^{-1}_{k+1,k}(v_{k+1}-v_k)\right)+\partial_x\left(m_yH\Delta^{-1}_{k+1,k}(u_{k+1}v_{k+1}-u_kv_k)\right)+\partial_y\left(m_xH\Delta^{-1}_{k+1,k}(v_{k+1}v_{k+1}-v_kv_k)\right)$$
$$+m\Delta^{-1}_{k+1,k}\left(\Delta^{-1}_{k+1}\left((wv)_{k+1}-(wv)_k\right)-\Delta^{-1}_k\left((wv)_k-(wv)_{k-1}\right)\right)$$
$$+\Delta^{-1}_{k+1,k}\left((mf+v_{k+1}\partial_xm_y-u_{k+1}\partial_ym_x)Hu_{k+1}-(mf+v_k\partial_xm_y-u_k\partial_ym_x)Hu_k\right)$$
$$=m_xH\Delta^{-1}_{k+1,k}g(b_{k+1}-b_k)(\partial_xh-z_k\partial_xH)-0.5m_xH^2\Delta^{-1}_{k+1,k}g(\Delta_{k+1}\partial_xb_{k+1}+\Delta_k\partial_xb_k)$$
$$+m\Delta^{-1}_{k+1,k}\left(\Delta^{-1}_{k+1}\left((\tau_{yz})_{k+1}-(\tau_{yz})_k\right)-\Delta^{-1}_k\left((\tau_{yz})_k-(\tau_{yz})_{k-1}\right)\right)+\Delta^{-1}_{k+1,k}\left((Q_v)_{k+1}-(Q_v)_k\right) \quad (31)$$

$$\Delta_{k+1,k}=0.5(\Delta_{k+1}+\Delta_k) \quad (32)$$

Inspection of equations (30,31) reveals that they could have also been obtained by differentiating the horizontal momentum equations (16,17) with respect to z and introducing a finite difference discretion in z. Using equations (20,21) to relate the shear stresses to the velocity differences across the interior interfaces suggest that equations (30,31) be interpreted as a system of K-1 equations for either the K-1 interfacial velocity differences or the K-1 interior interfacial shear stresses. Details of the solution of the internal mode equations (30,31) will be presented in Section 5.

The solution of the vertical velocity, w, employs the continuity equations. Dividing equation (23) by Δk, and subtracting equation (26) gives:

$$w_k=w_{k-1}-m^{-1}\Delta_k\left(\partial_x\left(m_yH(u_k-\bar{u})\right)+\partial_y\left(m_xH(v_k-\bar{v})\right)\right) \quad (33)$$

Since $w_o = 0$, the solution proceeds from the first cell layer to the surface. Provided the constraints (28,29) are satisfied, the surface velocity at k = K will be zero and satisfy the boundary condition.

4. COMPUTATIONAL ASPECTS OF THE EXTERNAL MODE SOLUTION

The formulation of a computational algorithm for the numerical solution of the external mode equations (24-26) begins by introducing modified variables and reorganizing the equations to give:

$$\partial_t \overline{U} = -m_x^{-1} m_y H g \partial_x \zeta - m_x^{-1} m_y H \partial_x p_s + m_x^{-1} m_y H g\left(\overline{b}\,\partial_x h - \overline{B}\,\partial_x H - 0.5 H \partial_x \overline{\beta}\right)$$
$$-m_x^{-1}\sum_{k=1}^{K}\Delta_k\left(\partial_x(U_k u_k) + \partial_y(V_k u_k)\right) + m_x^{-1}\sum_{k=1}^{K}\Delta_k(mf + v_k\partial_x m_y - u_k\partial_y m_x)Hv_k$$
$$+m_y(\tau_{xz})_K - m_y(\tau_{xz})_0 + m_x^{-1}\overline{Q}_u \tag{34}$$

$$\partial_t \overline{V} = -m_x m_y^{-1} H g \partial_y \zeta - m_x m_y^{-1} H \partial_y p_s + m_x m_y^{-1} H g\left(\overline{b}\,\partial_y h - \overline{B}\,\partial_y H - 0.5 H \partial_y \overline{\beta}\right)$$
$$-m_y^{-1}\sum_{k=1}^{K}\Delta_k\left(\partial_x(U_k v_k) + \partial_y(V_k v_k)\right) - m_y^{-1}\sum_{k=1}^{K}\Delta_k(mf + v_k\partial_x m_y - u_k\partial_y m_x)Hu_k$$
$$+m_x(\tau_{yz})_K - m_x(\tau_{yz})_0 + m_y^{-1}\overline{Q}_v \tag{35}$$

$$\partial_t \zeta + m^{-1}\left(\partial_x \overline{U} + \partial_y \overline{V}\right) = 0 \tag{36}$$

$$\overline{U} = m_y H \overline{u} \tag{37}$$

$$\overline{V} = m_x H \overline{v} \tag{38}$$

$$U_k = m_y H u_k \tag{39}$$

$$V_k = m_x H v_k \tag{40}$$

$$\overline{\beta} = \left(\sum_{k=1}^{K}\Delta_k \beta_k\right) \tag{41}$$

$$\overline{B} = \left(\sum_{k=1}^{K}\left(\Delta_k \beta_k + 0.5\Delta_k(z_k + z_{k-1})b_k\right)\right) \tag{42}$$

Equations (34,35) now equate the time rate of change of the external or depth integrated volumetric transports to the pressure gradients associated with the free surface slope, atmospheric pressure and buoyancy, the advective accelerations, the Coriolis and curvature accelerations, the free surface and bottom tangential stresses and the general source, sink terms. The staggered location of variables on the computational grid, Figure 2, allows most horizontal spatial derivatives in equations (34-36) to be represented by second order accurate central differences and results in conservation of volume, mass, momentum and energy in the limit of exact integration of the equations in time (Simons, 1973, Haltiner and Williams, 1980). When a variable is not located at a point required for implementation of central difference operators, averaging in either or both spatial directions is appropriate. The use of the spatial averaging scheme of Arakawa and Lamb (1977) to represent the Coriolis and curvature accelerations also guarantees energy conservation.

Following the introduction of discrete finite difference and averaging representations in space, equations (34-36), for a horizontal grid of L cells, may be viewed as a system of 3L ordinary differential equations in time for the volumetric transport and the free surface displacement. The numerous techniques available to solve these equations generally fall within the two categories of explicit and semi-implicit. The most frequently used explicit scheme is the three time level leapfrog scheme where the time derivatives are approximated between time levels n+1 and n-1, and the remaining terms are evaluated at time level n. Although computationally simple to implement, the maximum time step is restricted by the Courant-Fredrick-Levy condition based on the gravity wave phase speed. An alternate approach allowing larger time steps is the semi-implicit three time level scheme (Madala and

Piacsek, 1977), which when implemented for equations (34-36) is

$$\bar{U}^{n+1} = \bar{U}^{n-1} - \theta(m_x^{-1}m_yH)^u g\delta_x^u\left(\zeta^{n+1}+\zeta^{n-1}\right) - 2\theta(m_x^{-1}m_yH)^u\delta_x^u p_s$$
$$+2\theta(m_x^{-1}m_yH)^u g\left(\bar{b}^u\delta_x^u h - \bar{B}^u\delta_x^u H - 0.5H^u\delta_x^u\bar{\beta}\right) - 2\theta(m_x^{-1})^u\sum_{k=1}^{K}\Delta_k\left(\delta_x^u(U_ku_k)+\delta_y^u(V_ku_k)\right)$$
$$+2\theta(m_x^{-1})^u\sum_{k=1}^{K}\Delta_k\left((mf+v_k\partial_x m_y - u_k\partial_y m_x)Hv_k\right)^u + 2\theta m_y^u\left((\tau_{xx}^{n-1})_K - (\tau_{xx}^{n-1})_0\right)^u$$
$$+2\theta(m_x^{-1})^u\sum_{k=1}^{K}\Delta_k\left(\partial_x\left(m_yH\tau_{xx}^{n-1}\right)+\partial_y\left(m_xH\tau_{xy}^{n-1}\right)+\partial_y m_xH\tau_{xy}^{n-1}-\partial_x m_yH\tau_{yy}^{n-1}\right)_k^u \qquad (43)$$

$$\bar{V}^{n+1} = \bar{V}^{n-1} - \theta(m_xm_y^{-1}H)^v g\delta_y^v\left(\zeta^{n+1}+\zeta^{n-1}\right) - 2\theta(m_xm_y^{-1}H)^v\delta_y^v p_s$$
$$+2\theta(m_xm_y^{-1}H)^v g\left(\bar{b}^v\delta_y^v h - \bar{B}^v\delta_y^v H - 0.5H^v\delta_y^v\bar{\beta}\right) - 2\theta(m_y^{-1})^v\sum_{k=1}^{K}\Delta_k\left(\delta_x^v(U_kv_k)+\delta_y^v(V_kv_k)\right)$$
$$-2\theta(m_y^{-1})^v\sum_{k=1}^{K}\Delta_k\left((mf+v_k\partial_x m_y - u_k\partial_y m_x)Hu_k\right)^v + 2\theta m_x^v\left((\tau_{yx}^{n-1})_K - (\tau_{yx}^{n-1})_0\right)^v$$
$$+2\theta(m_y^{-1})^v\sum_{k=1}^{K}\Delta_k\left(\partial_x\left(m_yH\tau_{yx}^{n-1}\right)+\partial_y\left(m_xH\tau_{yy}^{n-1}\right)-\partial_y m_xH\tau_{xx}^{n-1}+\partial_x m_yH\tau_{yx}^{n-1}\right)_k^v \qquad (44)$$

$$\zeta^{n+1} - \zeta^{n-1} + \theta(m^{-1})^\zeta\left(\delta_x^\zeta(\bar{U}^{n+1}+\bar{U}^{n-1})+\delta_y^\zeta(\bar{V}^{n+1}+\bar{V}^{n-1})\right) = 0 \qquad (45)$$

with θ being the time step. All terms in equations (43-45) are understood to be evaluated at the center time level n except those evaluated at the forward and backward time levels, n+1 and n-1, which are denoted by superscripts. The u, v, and ζ superscripts indicate that a variable is evaluated, or that a spatial derivative is centered, at the corresponding spatial point.

The subscript of the spatial central difference operator, δ, indicates direction. The grid cells are presumed to be bounded in the horizontal by lines of constant integer values of the dimensionless orthogonal coordinates x and y, resulting in the central spatial differences having the forms:

$$\delta_x(\phi(x,y)) = \phi(x+0.5,y) - \phi(x-0.5,y) \qquad (46)$$

$$\delta_y(\phi(x,y)) = \phi(x,y+0.5) - \phi(x,y-0.5) \tag{47}$$

Application of these finite difference operators to the advective accelerations is illustrated by:

$$\delta_x^u(U_k(x)u_k(x)) = U_k(x+0.5)u_k(x+0.5) - U_k(x-0.5)u_k(x-0.5) \tag{48}$$

where the constant y dependence of the variables is implied. Since the u type variables are located at integer values of x, averaging is necessary to obtain values at the half intervals. Averaging both the transport and the velocity gives:

$$\begin{aligned}\delta_x^u(U_k(x)u_k(x)) &= 0.25(U_k(x+1)+U_k(x))(u_k(x+1)+u_k(x)) \\ &-0.25(U_k(x)+U_k(x-1))(u_k(x)+u_k(x-1))\end{aligned} \tag{49}$$

which is consistent with a central difference approximation of the nonconservative form of this portion of the advective acceleration. Averaging the transport and allowing the velocity to be advected from the upwind direction gives:

$$\begin{aligned}\delta_x^u(U_k(x)u_k(x)) &= 0.5Max((U_k(x+1)+U_k(x)),0)u_k^{n-1}(x,y) \\ &+0.5Min((U_k(x+1)+U_k(x)),0)u_k^{n-1}(x+1,y) \\ &-0.5Max((U_k(x)+U_k(x-1)),0)u_k^{n-1}(x-1,y) \\ &-0.5Min((U_k(x)+U_k(x-1)),0)u_k^{n-1}(x,y)\end{aligned} \tag{50}$$

which is consistent with an upwind or backward difference approximation of the nonconservative form of this portion of the advective acceleration. In equation (50), the transport is still at time level n, while the velocity is at time level n-1, for both stability and accuracy (Smolarkiewicz and Clark, 1986). The preference for the use of equation (49) or equation (50) will generally depend upon the physical situation being simulated. The central difference form introduces no numerical diffusion but may produce solution fields which exhibit cell to cell spatial oscillations. These oscillations can be

eliminated by the addition of horizontal diffusion terms to the momentum equations. Specification of the horizontal diffusivity allows the degree of spatial smoothing to be controlled. The upwind difference form introduces numerical diffusion and does not produce spatial oscillations in the solution field. The Coriolis and curvature terms in equations (43,44) are discretized using an energy conserving spatial averaging and differencing (Arakawa and Lamb ,1977, Haltiner and Williams, 1980). For example, the Coriolis and curvature term in equation (43) is given by:

$$\left((mf + v_k\partial_x m_y - u_k\partial_y m_x)Hv_k\right)^{\kappa} = 0.5\left(\left(RHv_k\right)^{\zeta}(x+0.5,y) + \left(RHv_k\right)^{\zeta}(x-0.5,y)\right) \tag{51}$$

$$R_k^{\zeta}(x+0.5) = fm(x+0.5,y) + v_k^{\zeta}(x+0.5,y)\left(m_y(x+1,y) - m_y(x,y)\right)$$
$$-u_k^{\zeta}(x+0.5,y)\left(m_x(x+0.5,y+0.5) - m_x(x+0.5,y-0.5)\right) \tag{52}$$

$$v_k^{\zeta}(x+0.5,y) = 0.5\left(v_k(x+0.5,y+0.5) + v_k(x+0.5,y-0.5)\right) \tag{53}$$

$$u_k^{\zeta}(x+0.5,y) = 0.5\left(u_k(x+1,y) + u_k(x,y)\right) \tag{54}$$

where the variables locations are shown in Figure 3.

Since the bottom tangential stresses in equations (43,44) must be supplied from the internal mode solution which follows the external solution, it is lagged at the backward time level. The general source, sink term has been replaced by horizontal diffusion terms having the form proposed by Mellor and Blumberg (1985). The horizontal stress tensor is taken of the form:

$$\left(\tau_{xx}\right)_k = 2A_H m_x^{-1}\partial_x u_k \tag{55}$$

$$\left(\tau_{xy}\right)_k = \left(\tau_{yx}\right)_k = 2A_H\left(m_x^{-1}\partial_x v_k + m_y^{-1}\partial_y u_k\right) \tag{56}$$

$$\left(\tau_{yy}\right)_k = 2A_H m_y^{-1}\partial_y v_k \tag{57}$$

The horizontal diffusion coefficient, AH, is often specified as a minimum constant value necessary to smooth cell to cell spatial oscillations in the solution field when the central difference form of the advective acceleration, equation (49) is used. When the horizontal turbulent diffusion is used to represent subgrid scale mixing, AH may be determined as suggested by Smagorinsky (1963).

The solution scheme for equations (43-45) involves first evaluating all terms in the three equations at time levels n and n-1. On boundaries where the transports are specified, the specified values at time level n+1 are inserted into equation (45). Equations (43,44) are then used to eliminate the unknown transports at time level n+1, from equation (45). The result is a discrete Helmholtz type elliptic equation for the free surface displacement at time level n+1, having the general form:

$$\zeta^{n+1} - g\theta^2 (m^{-1})^{\zeta} \left(\delta_x^{\zeta} \left((m_x^{-1} m_y H)^u \delta_x^u \zeta^{n+1} \right) + \delta_y^{\zeta} \left((m_x m_y^{-1} H)^v \delta_y^v \zeta^{n+1} \right) \right) - \phi = 0 \qquad (58)$$

with the term ϕ containing all of the previously evaluated terms and transport boundary conditions. For cells where the free surface displacement is specified, equation (58) is replaced by an equation which enforces the specified boundary condition at time level n+1. For the rigid lid case where the free surface displacement is constant in time and space, equation (58) is modified to give an equation for the unknown surface pressure, ps, by eliminating the first term, replacing $g\zeta$ in the discrete elliptic operator by ps, and appropriately modifying the last term. In the computer code, the system of equations corresponding to equation (58) is solved by a reduced system conjugate gradient scheme with a multicolor or red-black ordering of the cells (Hageman and Young, 1981). The conjugate gradient iterations continue until the sum of the squared residuals is less than a specified value. The free surface displacements or surface pressures are then substituted into equations (43,44) to determine the transports at time level n+1. Since the solution of equation (58) is approximate, equation (45) may not be identically

satisfied upon substitution of the time level n+1 transports and free surface displacement. To insure that equation (45) is identically satisfied in the case of a dynamic free surface, it is solved for a revised value of the time level n+1, free surface displacement after introduction of the time level n+1 transports. For the rigid lid case, an external divergence error is calculated and compensated for adding appropriate a volumetric source or sink terms to equation (45) during the next time step.

Some insight into the stability and accuracy of the semi-implicit three time level scheme for solving the external mode equations with a dynamically active free surface can be gained by a Fourier analysis of the linearized discrete equations:

$$\overline{U}^{n+1} = \overline{U}^{n-1} - \theta(m_x^{-1}m_y h_o)^u g\delta_x^u\left(\zeta^{n+1}+\zeta^{n-1}\right)+2\theta(m_x^{-1}m_y)^u f\overline{V}^u \tag{59}$$

$$\overline{V}^{n+1} = \overline{V}^{n-1} - \theta(m_x m_y^{-1}h_o)^v g\delta_y^v\left(\zeta^{n+1}+\zeta^{n-1}\right)-2\theta(m_x m_y^{-1})^v f\overline{U}^v \tag{60}$$

$$\zeta^{n+1} - \zeta^{n-1} + \theta(m^{-1})^\zeta\left(\delta_x^\zeta(\overline{U}^{n+1}+\overline{U}^{n-1})+\delta_y^\zeta(\overline{V}^{n+1}+\overline{V}^{n-1})\right)=0 \tag{61}$$

Introduction of the Fourier representations:

$$\begin{Bmatrix}\overline{U}\\ \overline{V}\\ \overline{W}\end{Bmatrix} = \begin{Bmatrix}U_o\\ V_o\\ W_o\end{Bmatrix}\exp\left(i\omega n\theta + ik_x m_x x + ik_y m_y y\right) \tag{62}$$

$$\overline{W} = \sqrt{gh_o m}\,\zeta \tag{63}$$

on a rectangular Cartesian grid gives the eigenvalue problem:

$$\lambda^2\mathbf{M}_+ + \lambda\mathbf{M} + \mathbf{M}_- = \mathbf{0} \tag{64}$$

$$\mathbf{M}_{+}=\begin{bmatrix} 1 & 0 & 2im_x^{-1}m_yC\sin(0.5k_xm_x) \\ 0 & 1 & 2im_xm_y^{-1}C\sin(0.5k_ym_y) \\ 2iC\sin(0.5k_xm_x) & 2iC\sin(0.5k_ym_y) & 1 \end{bmatrix} \tag{65}$$

$$\mathbf{M}=2f\theta\cos(0.5k_xm_x)\cos(0.5k_ym_y)\begin{bmatrix} 0 & -m_x^{-1}m_y & 0 \\ m_xm_y^{-1} & 0 & 0 \\ 0 & 0 & 0 \end{bmatrix} \tag{66}$$

$$\mathbf{M}_{-}=\begin{bmatrix} -1 & 0 & 2im_x^{-1}m_yC\sin(0.5k_xm_x) \\ 0 & -1 & 2im_xm_y^{-1}C\sin(0.5k_ym_y) \\ 2iC\sin(0.5k_xm_x) & 2iC\sin(0.5k_ym_y) & -1 \end{bmatrix} \tag{67}$$

$$C=\frac{\sqrt{gh_o}}{\sqrt{m}}\theta \tag{68}$$

where ω is the frequency, k_x and k_y are the wave numbers and C is the Courant number associated with the shallow water wave speed.

The eigenvalue, λ, is related to the frequency and time step by:

$$\lambda=|\lambda|\exp(i\omega\theta) \tag{69}$$

The characteristic polynomial of equation (64) is:

$$(\lambda^2-1)(\lambda^4-2\psi\lambda^2+1)=0 \tag{70}$$

$$\psi=\frac{1-4C^2\left(\frac{m_y}{m_x}\sin^2\left(\frac{k_xm_x}{2}\right)+\frac{m_x}{m_y}\sin^2\left(\frac{k_ym_y}{2}\right)\right)-2f^2\theta^2\cos^2\left(\frac{k_xm_x}{2}\right)\cos^2\left(\frac{k_ym_y}{2}\right)}{1+4C^2\left(\frac{m_y}{m_x}\sin^2\left(\frac{k_xm_x}{2}\right)+\frac{m_x}{m_y}\sin^2\left(\frac{k_ym_y}{2}\right)\right)} \tag{71}$$

and the roots or eigenvalues are:

$$\lambda = 1, \sqrt{\psi + i\sqrt{1-\psi^2}}, \sqrt{\psi - i\sqrt{1-\psi^2}}, -1, -\sqrt{\psi + i\sqrt{1-\psi^2}}, -\sqrt{\psi - i\sqrt{1-\psi^2}} \qquad (72)$$

For linear stability, the absolute values of the eigenvalues must be less than or equal to one. The absolute values of the four complex eigenvalues are identically one, provided the absolute value of ψ is less than one, which requires:

$$\theta \leq |f|^{-1} \qquad (73)$$

Thus the linearized three time level semi-implicit scheme is neutrally stable when equation (73) is satisfied. Since at mid-latitude the inverse of the Coriolis parameter is on the order of 10,000 sec, the time step is not overly constrained. The overall stability of the scheme will most likely be controlled by the stability of the explicit advective and curvature accelerations. The form of the curvature terms in the momentum equations suggest that they may increase the effective magnitude of the Coriolis parameter and reduce the stable time step. The stability of the explicit scheme for the advective accelerations will be discussed in subsequent sections. The major computational problem with three time level schemes for systems of first order equations is the doubling of the number of eigenvalues over those physically characterizing the system. The eigenvalues in equation (72) are grouped such that the first three correspond to the true physical solution or physical mode of the system while the last three are spurious and give rise to what is referred to as the computational mode (Haltiner and Williams, 1980). Expressing the physical mode eigenvalues of the numerical scheme in terms of $\omega\theta$, using equation (69), gives the dispersion relation:

$$\omega\theta = 0, \pm 0.5 \arccos(|\psi|) \qquad (74)$$

which can be compared with the dispersion relation

$$\omega\theta = 0, \pm\sqrt{f^2\theta^2 + m_x^{-1}m_y\left(Ck_x m_x\right)^2 + m_x m_y^{-1}\left(Ck_y m_y\right)^2} \tag{75}$$

for the continuous in time and space form of equations (59-61). Both the numerical and continuous solution are characterized by a steady mode and pairs of waves propagating in opposite directions. The major feature of the computational mode of the numerical solution scheme, represented by the last three eigenvalues in equation (72), is an alternating change in sign of the solution at every time step. Since all eigenvalues of the scheme are neutrally stable, the computational mode solution can persist and become a source of error. Two alternatives to eliminating the computational mode are the application of weak time filter or the periodic insertion of a single step using a two time level scheme (Haltiner and Williams, 1980). For the present work, the insertion of a two time level step or possibly more appropriately termed a correction step was selected.

The correction step used to eliminate the computational mode is a trapezoidal scheme. The scheme computes a corrected time level n+1 solution using the initial condition at time level n and the solution at time level n+1 previously computed using the three time level scheme. The momentum and continuity equations, equivalent to equations (43-45), for the trapezoidal correction step are:

$$\begin{aligned}
&\overline{U}^{n+1} = \overline{U}^{n} - 0.5\theta(m_x^{-1}m_y H^{n+\frac{1}{2}})^{u} g\delta_x^{u}\left(\zeta^{n+1} + \zeta^{n}\right) - \theta\left((m_x^{-1}m_y H)^{u}\delta_x^{u} p_s\right)^{n+\frac{1}{2}} \\
&+\theta\left((m_x^{-1}m_y H)^{u} g\left(\overline{b}^{u}\delta_x^{u} h - \overline{B}^{u}\delta_x^{u} H - 0.5H^{u}\delta_x^{u}\overline{\beta}\right)\right)^{n+\frac{1}{2}} - \theta(m_x^{-1})^{u}\sum_{k=1}^{K}\Delta_k\left(\delta_x^{u}(U_k u_k) + \delta_y^{u}(V_k u_k)\right) \\
&+\theta(m_x^{-1})^{u}\sum_{k=1}^{K}\Delta_k\left(\left((mf + v_k\partial_x m_y - u_k\partial_y m_x)Hv_k\right)^{u}\right)^{n+\frac{1}{2}} + \theta m_y^{u}\left((\tau_{xx}^{n})_K - (\tau_{xx}^{n})_0\right)^{u} \\
&+\theta(m_x^{-1})^{u}\sum_{k=1}^{K}\Delta_k\left(\partial_x\left(m_y H\tau_{xx}^{n}\right) + \partial_y\left(m_x H\tau_{xy}^{n}\right) + \partial_y m_x H\tau_{xy}^{n} - \partial_x m_y H\tau_{yy}^{n}\right)_k^{u}
\end{aligned} \tag{76}$$

$$\bar{V}^{n+1} = \bar{V}^n - 0.5\theta(m_x m_y^{-1} H^{n+\frac{1}{2}})^v g\delta_y^v\left(\zeta^{n+1} + \zeta^n\right) - \theta\left((m_x m_y^{-1} H)^v \delta_y^v p_s\right)^{n+\frac{1}{2}}$$

$$+\theta\left((m_x m_y^{-1} H)^v g\left(\bar{b}^v \delta_y^v h - \bar{B}^v \delta_y^v H - 0.5 H^v \delta_y^v \bar{\beta}\right)\right)^{n+\frac{1}{2}} - \theta(m_y^{-1})^v \sum_{k=1}^{K} \Delta_k\left(\delta_x^v (U_k v_k) + \delta_y^v (V_k v_k)\right)$$

$$-\theta(m_y^{-1})^v \sum_{k=1}^{K} \Delta_k\left(\left((mf + v_k \partial_x m_y - u_k \partial_y m_x) H u_k\right)^v\right)^{n+\frac{1}{2}} + \theta m_x^v\left((\tau_{yz}^n)_K - (\tau_{yz}^n)_0\right)^v$$

$$+\theta(m_y^{-1})^v \sum_{k=1}^{K} \Delta_k\left(\partial_x\left(m_y H \tau_{yx}^n\right) + \partial_y\left(m_x H \tau_{yy}^n\right) - \partial_y m_x H \tau_{xx}^n + \partial_x m_y H \tau_{yx}^n\right)_k^v \qquad (77)$$

$$\zeta^{n+1} - \zeta^n + 0.5\theta(m^{-1})^\zeta\left(\delta_x^\zeta(\bar{U}^{n+1} + \bar{U}^n) + \delta_y^\zeta(\bar{V}^{n+1} + \bar{V}^n)\right) = 0 \qquad (78)$$

where the notation n+1/2 implies:

$$(\ )^{n+\frac{1}{2}} = 0.5\left((\ )^* + (\ )^n\right)$$

with * denoting evaluation using time level n+1 results from the previous three time level step. Because of stability restrictions, the advective accelerations must be of the upwind form:

$$\delta_x^u\left(U_k(x) u_k(x)\right) = 0.5 Max\left(\left(U_k(x+1) + U_k(x)\right), 0\right)^{n+\frac{1}{2}} u_k^n(x,y)$$

$$+0.5 Min\left(\left(U_k(x+1) + U_k(x)\right), 0\right)^{n+\frac{1}{2}} u_k^n(x+1,y)$$

$$-0.5 Max\left(\left(U_k(x) + U_k(x-1)\right), 0\right)^{n+\frac{1}{2}} u_k^n(x-1,y)$$

$$-0.5 Min\left(\left(U_k(x) + U_k(x-1)\right), 0\right)^{n+\frac{1}{2}} u_k^n(x,y) \qquad (79)$$

The solution of semi-implicit equations (76-78) follows that outlined for the three time level scheme.

To analyze the stability of the trapezoidal correction step with a dynamically active free surface, two points of view will be considered. Since a single application of the trapezoidal scheme essentially corrects a step of the three time level scheme, it is actually three time level. The Fourier analysis of the combined

linearized three time level, trapezoidal correction scheme on a rectangular Cartesian grid gives the eigenvalue problem:

$$\lambda^2 \mathbf{N}_+ + \lambda(\mathbf{N} + \mathbf{N}_- - \mathbf{N}\mathbf{M}_+^{-1}\mathbf{M}) - \mathbf{N}\mathbf{M}_+^{-1}\mathbf{M}_- = \mathbf{0} \tag{80}$$

$$\mathbf{N}_+ = \begin{bmatrix} 1 & 0 & im_x^{-1}m_y C\sin(0.5k_x m_x) \\ 0 & 1 & im_x m_y^{-1} C\sin(0.5k_y m_y) \\ iC\sin(0.5k_x m_x) & iC\sin(0.5k_y m_y) & 1 \end{bmatrix} \tag{81}$$

$$\mathbf{N} = 0.5f\theta\cos(0.5k_x m_x)\cos(0.5k_y m_y)\begin{bmatrix} 0 & -m_x^{-1}m_y & 0 \\ m_x m_y^{-1} & 0 & 0 \\ 0 & 0 & 0 \end{bmatrix} \tag{82}$$

$$\mathbf{N}_- = \begin{bmatrix} -1 & 0 & im_x^{-1}m_y C\sin(0.5k_x m_x) \\ 0 & -1 & im_x m_y^{-1} C\sin(0.5k_y m_y) \\ iC\sin(0.5k_x m_x) & iC\sin(0.5k_y m_y) & -1 \end{bmatrix} \tag{83}$$

The sixth order characteristic polynomial of equation (80) is algebraically rather complex and only the two roots or eigenvalues, 1 and 0, can be determined in closed form. The eigenvalue of one is associated with the steady physical mode, while the eigenvalue of zero is spurious but serves a useful purpose in eliminating the computational mode. A second point of view is that the successive application of the trapezoidal correction is equivalent to an iterative two time level scheme. The Fourier analysis of such a scheme gives the eigenvalue problem:

$$\lambda(\mathbf{N}_+ + \mathbf{N}) + (\mathbf{N} + \mathbf{N}_-) = \mathbf{0} \tag{84}$$

whose characteristic polynomial is:

$$(\lambda - 1)(\lambda^2 - 2\chi\lambda + 1) = 0 \tag{85}$$

where

$$\chi = \frac{1 - C^2\left(\frac{m_y}{m_x}\sin^2\left(\frac{k_x m_x}{2}\right) + \frac{m_x}{m_y}\sin^2\left(\frac{k_y m_y}{2}\right)\right) - \frac{1}{4}f^2\theta^2\cos^2\left(\frac{k_x m_x}{2}\right)\cos^2\left(\frac{k_y m_y}{2}\right)}{1 + C^2\left(\frac{m_y}{m_x}\sin^2\left(\frac{k_x m_x}{2}\right) + \frac{m_x}{m_y}\sin^2\left(\frac{k_y m_y}{2}\right)\right) + \frac{1}{4}f^2\theta^2\cos^2\left(\frac{k_x m_x}{2}\right)\cos^2\left(\frac{k_y m_y}{2}\right)} \tag{86}$$

The roots or eigenvalues of equation (80) are:

$$\lambda = 1, \chi + i\sqrt{1-\chi^2}, \chi - i\sqrt{1-\chi^2} \ . \tag{87}$$

Since the absolute value of chi is always less than one, the absolute value of the complex eigenvalues is identically one and the scheme is neutrally and unconditionally stable.

The results of the Fourier analysis is also useful in accessing the accuracy of the external mode solution scheme with respect to its ability to represent the dispersion relation and the phase and group velocities of shallow water waves (Foreman, 1983). The dispersion relations for the continuous in space and time shallow water equations, and the three and two time level schemes, respectively, are:

$$\omega\theta = \sqrt{f^2\theta^2 + m_x^{-1}m_y\left(Ck_x m_x\right)^2 + m_x m_y^{-1}\left(Ck_y m_y\right)^2} \tag{88}$$

$$\omega\theta = 0.5\arccos(\psi) \tag{89}$$

$$\omega\theta = \arccos(\chi) \tag{90}$$

where ψ and χ are given by equations (71,86). The phase and group velocities are given respectively by:

$$\frac{(c_x, c_y)}{\sqrt{gh_o}} = \frac{(k_x, k_y)}{\sqrt{m\left(k_x^2 + k_y^2\right)}}\frac{\omega\theta}{C} \tag{91}$$

$$\frac{(G_x, G_y)}{\sqrt{gh_o}} = \frac{1}{\sqrt{m}}\left(\frac{\partial}{\partial k_x}, \frac{\partial}{\partial k_y}\right)\frac{\omega\theta}{C} \tag{92}$$

A comparison of the dispersion relations for a square Cartesian grid with a Courant number of 5 and $f\theta$ of 0.01 is shown in Figure 4. The dispersion relations for the three time level and the two time level, included for comparison, difference schemes show excellent agreement with the continuous equations for dimensionless wave numbers less than approximately 0.05. As the dimensionless wave number magnitude increases toward 0.1, both numerical schemes under predict the dimensionless frequency with the three time level scheme being less accurate than the two time level scheme. The magnitudes of the phase velocity as a function of the dimensionless horizontal wave numbers are shown in Figure 5. Both numerical schemes increasingly under predict the phase velocity magnitude as the wave number magnitude increases, but provide relatively accurate predictions for dimensionless magnitudes less than 0.05, with the two time level scheme being more accurate. The magnitudes of the group velocity as a function of the dimensionless horizontal wave numbers are shown in Figure 6. Again the numerical schemes increasingly under predict the group velocity magnitude as the wave number magnitude increases, but provide relatively accurate predictions for dimensionless magnitudes less than 0.05. Although the two time level scheme is shown to be more accurate than the three time level scheme at higher wave number magnitudes, it would be computationally much more costly to implement due to the iterative evaluation of the Coriolis, curvature and advective accelerations.

5. COMPUTATIONAL ASPECTS OF THE INTERNAL MODE SOLUTION

The internal mode equations (30,31) are solved using a fractional step scheme (Peyret and Taylor, 1983), with the first step being explicit and the second step being implicit. Figure 7 illustrates the location variables in the x,z plane for the x componoent of the internal mode equations. The computational equations for the three time level explicit step are:

$$
\begin{aligned}
&(U_{k+1}-U_k)^{**} = (U_{k+1}-U_k)^{n-1} - 2\theta(m_x^{-1})^u\left(\delta_x^u(U_{k+1}u_{k+1}-U_ku_k)+\delta_y^u(V_{k+1}u_{k+1}-V_ku_k)\right)\\
&-2\theta(m_x^{-1})^u\left(\Delta_{k+1}^{-1}((Wu)_{k+1}-(Wu)_k)-\Delta_k^{-1}((Wu)_k-(Wu)_{k-1})\right)^u\\
&+2\theta(m_x^{-1})^u\left((mf+v_{k+1}\partial_x m_y-u_{k+1}\partial_y m_x)Hv_{k+1}-(mf+v_k\partial_x m_y-u_k\partial_y m_x)Hv_k\right)^u\\
&+2\theta(m_x^{-1}m_yH)^u g\left((b_{k+1}-b_k)^u\delta_x^u(h-z_kH)-0.5H^u\delta_x^u(\Delta_{k+1}b_{k+1}+\Delta_kb_k)\right)\\
&+2\theta(m_x^{-1})^u\left((Q_u)_{k+1}-(Q_u)_k\right)^u
\end{aligned}
\tag{94}
$$

$$
\begin{aligned}
&(V_{k+1}-V_k)^{**} = (V_{k+1}-V_k)^{n-1} - 2\theta(m_y^{-1})^v\left(\delta_x^v(U_{k+1}v_{k+1}-U_kv_k)+\delta_y^v(V_{k+1}v_{k+1}-V_kv_k)\right)\\
&-2\theta(m_y^{-1})^v\left(\Delta_{k+1}^{-1}((Wv)_{k+1}-(Wv)_k)-\Delta_k^{-1}((Wv)_k-(Wv)_{k-1})\right)^v\\
&-2\theta(m_y^{-1})^v\left((mf+v_{k+1}\partial_x m_y-u_{k+1}\partial_y m_x)Hu_{k+1}-(mf+v_k\partial_x m_y-u_k\partial_y m_x)Hu_k\right)^v\\
&+2\theta(m_xm_y^{-1}H)^v g\left((b_{k+1}-b_k)^v\delta_y^v(h-z_kH)-0.5H^v\delta_y^v(\Delta_{k+1}b_{k+1}+\Delta_kb_k)\right)\\
&+2\theta(m_y^{-1})^v\left((Q_v)_{k+1}-(Q_v)_k\right)^v
\end{aligned}
\tag{95}
$$

$$
W = mw = m_xm_yw \tag{96}
$$

where ** denotes the provisional solution, and all terms not having a specified time level are understood to be at the centered time level n. The horizontal volume transports, U and V are as defined by equations (39,40) and W is the vertical volume transport. The horizontal difference operations on the horizontal advection terms are identical to those presented in Section 3, equations (48-50). The vertical momentum flux terms may be represented in forms

consistent with central or upwind differencing,

$$(Wu)_k^u = 0.25\big(W_k(x-0.5)+W_k(x+0.5)\big)\big(u_k(x)+u_{k+1}(x)\big) \tag{97}$$

$$(Wu)_k^u = 0.5Max\big(\big(W_k(x-0.5)+W_k(x+0.5)\big),0\big)u_k^{n-1}(x)$$
$$+0.5Min\big(\big(W_k(x-0.5)+W_k(x+0.5)\big),0\big)u_{k+1}^{n-1}(x) \tag{98}$$

where the advected velocity in the upwind form, equation (98) is evaluated at time level n-1 for stability. The horizontal difference operations on the buoyancy and mean and total depths are central difference operators defined by equations (46) and (47). The inclusion of horizontal diffusion in the source, sink terms in equations (94,95) would follow from its inclusion in equations (43,44). The Coriolis and curvature terms are averaged and differenced by the energy conserving scheme presented in Section 3, equations (51-53). The stability of the explicit fractional step, equations (94,95), is governed by the stability of the discretization of the horizontal and vertical advective accelerations, which will be discussed in Section 5, and the discretization of the Coriolis and curvature terms. The results of the Fourier stability analysis of the external mode scheme, with respect to the Coriolis acceleration, can be shown to apply to the internal mode scheme as well.

The computational equations for the second step of the three time level scheme are:

$$\frac{(U_{k+1}-U_k)^{n+1}}{2\theta m_y^u \Delta_{k+1,k}} = \frac{(U_{k+1}-U_k)^{**}}{2\theta m_y^u \Delta_{k+1,k}} + \left(\frac{((\tau_{xz})_{k+1}-(\tau_{xz})_k)}{\Delta_{k+1}\Delta_{k+1,k}} - \frac{((\tau_{xz})_k-(\tau_{xz})_{k-1})}{\Delta_k\Delta_{k+1,k}}\right)^{n+1} \tag{99}$$

$$\frac{(V_{k+1}-V_k)^{n+1}}{2\theta m_x^v \Delta_{k+1,k}} = \frac{(V_{k+1}-V_k)^{**}}{2\theta m_x^v \Delta_{k+1,k}} + \left(\frac{((\tau_{yz})_{k+1}-(\tau_{yz})_k)}{\Delta_{k+1}\Delta_{k+1,k}} - \frac{((\tau_{yz})_k-(\tau_{yz})_{k-1})}{\Delta_k\Delta_{k+1,k}}\right)^{n+1} \tag{100}$$

Using equations (20,21), the turbulent shear stresses are related to

the horizontal transports by:

$$(\tau_{xz})_k^{n+1} = \left(\frac{A_v^u}{H^u}\right)_k^n \left(\frac{U_{k+1} - U_k}{m_y^u H^u \Delta_{k+1,k}}\right)^{n+1} \tag{101}$$

$$(\tau_{yz})_k^{n+1} = \left(\frac{A_v^v}{H^v}\right)_k^n \left(\frac{V_{k+1} - V_k}{m_x^v H^v \Delta_{k+1,k}}\right)^{n+1} \tag{102}$$

Equations (101,102) could be used to eliminate the turbulent shear stresses from equations (99,100) to give a pair of K-1 systems of equations for the transport differences between layers, however, the resulting equations are poorly conditioned. Instead, equations (101,102) are used to eliminate the horizontal transport differences at time level n+1 from equations (99,100) to give a pair of K-1 equations for the turbulent shear stresses

$$-\Delta_k^{-1}\Delta_{k+1,k}^{-1}(\tau_{xz})_{k-1}^{n+1} + \left(\Delta_k^{-1}\Delta_{k+1,k}^{-1} + \frac{(H^u)^{n+1}}{2\theta}\left(\frac{H^u}{A_v^u}\right)_k^n + \Delta_{k+1}^{-1}\Delta_{k+1,k}^{-1}\right)(\tau_{xz})_k^{n+1} - \Delta_{k+1}^{-1}\Delta_{k+1,k}^{-1}(\tau_{xz})_{k+1}^{n+1}$$
$$= \left(2\theta m_y^u \Delta_{k+1,k}\right)^{-1}(U_{k+1} - U_k)^{**} \tag{103}$$

$$-\Delta_k^{-1}\Delta_{k+1,k}^{-1}(\tau_{yz})_{k-1}^{n+1} + \left(\Delta_k^{-1}\Delta_{k+1,k}^{-1} + \frac{(H^v)^{n+1}}{2\theta}\left(\frac{H^v}{A_v^v}\right)_k^n + \Delta_{k+1}^{-1}\Delta_{k+1,k}^{-1}\right)(\tau_{yz})_k^{n+1} - \Delta_{k+1}^{-1}\Delta_{k+1,k}^{-1}(\tau_{yz})_{k+1}^{n+1}$$
$$= \left(2\theta m_x^v \Delta_{k+1,k}\right)^{-1}(V_{k+1} - V_k)^{**} \tag{104}$$

These equations are diagonally dominant and well conditioned, and can be solved independently at each of the horizontal velocity locations. Since equations (103,104) represent fully implicit, backward difference in time, schemes for one dimensional parabolic diffusion equations, the solutions are unconditionally stable (Fletcher, 1988). Given the solutions of equations (103,104) the shear stresses, the K-1 transport differences, Uk+1-Uk and Vk+1-Vk, are determined from equations (101,102) and combined with the continuity constraints, equations (28,29), to form a pair of K equations for the

horizontal transports in each cell layer. To illustrate, the horizontal transports in the surface cell layer are determined analytically and given by:

$$U_K = \overline{U} + \sum_{k=1}^{K-1}\left(\sum_{j=1}^{k}\Delta_j\right)(U_{k+1} - U_k) \tag{105}$$

and a similar expression for VK. Working down from the surface using the K-1 transport differences allows the remaining transports to be determined. It is noted for later use that the bottom cell layer transports can be expressed in terms of the depth integrated transports and the transport differences using:

$$U_1 = \overline{U} - \sum_{k=1}^{K-1}\left(1 - \sum_{j=1}^{k}\Delta_j\right)(U_{k+1} - U_k) \tag{106}$$

and an identical equation for V1.

Solution of equations (103,104) requires specification of bottom and surface stresses at k=0 and k=K, respectively. On the free surface, k=K, the surface wind stress components are specified. On the bottom fluid-solid boundary, k=0, the bottom stress must be specified. The simplest approach to specifying the bottom stress components utilizes the velocity component in the bottom cell layer and the quadratic friction relations:

$$(\tau_{xz})_0^{n+1} = c_b\left(\sqrt{u_1 u_1 + v_1^u v_1^u}\right)^n\left(\frac{U_1}{m_y^u H^u}\right)^{n+1} \tag{107}$$

$$(\tau_{yz})_0^{n+1} = c_b\left(\sqrt{u_1^v u_1^v + v_1 v_1}\right)^n\left(\frac{V_1}{m_x^v H^v}\right)^{n+1} \tag{108}$$

Assuming a logarithmic velocity profile between the solid bottom and the middle of the bottom cell layer gives the bottom stress coefficient:

$$c_b = \kappa^2 \left(\ln\left(\frac{\Delta_1 H}{2 z_0^*} \right) \right)^{-2} \tag{109}$$

where z_0^* is the dimensional bottom roughness height. Inserting equation (106) and a corresponding equation for V_1 into equations (107,108), respectively allows the bottom stresses at time level n+1 to be expressed in terms of the depth integrated transport components, known from the external mode solution, and the unknown transport differences at time level n+1. However, the transport differences at time level n+1 are related to the shear stress components by equations (101,102), allowing the bottom stresses to be expressed in terms of the depth integrated transports and the internal shear stresses by:

$$(\tau_{xz})_0^{n+1} = c_b \left(\sqrt{u_1 u_1 + v_1^u v_1^u} \right)^n \left(\left(\frac{\overline{U}}{m_y^u H^u} \right)^{n+1} - \sum_{k=1}^{K-1} \left(1 - \sum_{j=1}^{k} \Delta_j \right) \frac{\Delta_{k+1,k} (\tau_{xz})_k^{n+1}}{\left(\frac{A_v^u}{H^u} \right)_k^n} \right) \tag{110}$$

and a similar expression for the y component. Inserting equation (110) and the corresponding y component equation for the bottom stress components into the k=1 pair of equations (103,104) results in a nearly tridiagonal system with a fully populated first row. The systems of equations are still efficiently solved using a tridiagonal equation solver and the Sherman-Morrison formula (Press *et al*, 1986).

The internal mode solution is completed by the determination of the vertical velocity using:

$$w_k = w_{k-1} - (m^\zeta)^{-1} \Delta_k \left(\delta_x^\zeta \left(U_k - \overline{U} \right) + \delta_y^\zeta \left(V_k - \overline{V} \right) \right) \tag{111}$$

which follows from equation (33). The solution of equation (111), where all variables are at time level n+1, proceeds from k=1 since $w_0=0$. A two time level correction step is also periodically inserted into the internal mode time integration on the same time step as the external mode correction. Since the computational equations follow directly from the three time level equations using the details of the external mode presentation in Section 4, they will not be presented here.

6. Numerical Solution Techniques for the Transport Equations

In this section, solutions techniques for the transport equations for salinity, temperature, turbulence intensity and turbulence length scale are presented. Stability and accuracy aspects of the advection schemes common to the transport equations and the external and internal horizontal momentum equations are also discussed. The salinity transport equation (8) is used as a generic example and the location of variables is shown in Figure 8.

The salinity transport equation (8) is integrated over a cell layer to give:

$$\partial_t(mHS_k)+\partial_x(U_kS_k)+\partial_y(V_kS_k)+\Delta_k^{-1}\left((WS)_k+(WS)_{k-1}\right)$$
$$-\Delta_k^{-1}m\left((H^{-1}A_b\partial_zS)_k-(H^{-1}A_b\partial_zS)_{k-1}\right)-(Q_S)_k=0 \qquad (112)$$

where Uk, Vk, and W are defined by equations (39,40,96). The source, sink, advection, and vertical diffusion portions of equation (112) are treated in separate fractional steps, as was done for the internal mode momentum equations in Section 5. The three time level fractional step sequence is given by:

$$S_k^*=S_k^{n-1}+2\theta(mH^{n-1})^{-1}(Q_S)_k^{n-1} \qquad (113)$$

$$(mH)^{n+1}S_k^{**} = (mH)^{n-1}S_k^{*} - 2\theta\left(\delta_x^{\zeta}(U_kS_k) + \delta_y^{\zeta}(V_kS_k) + \Delta_k^{-1}\left((WS)_k - (WS)_{k-1}\right)\right) \tag{114}$$

$$(HS_k)^{n+1} - 2\theta\left(\left(\frac{(H^{-1}A_b)_k^{n}(S_{k+1} - S_k)^{n+1}}{\Delta_k\Delta_{k+1,k}}\right) - \left(\frac{(H^{-1}A_b)_{k-1}^{n}(S_k - S_{k-1})^{n+1}}{\Delta_k\Delta_{k,k-1}}\right)\right) = H^{n+1}S_k^{**} \tag{115}$$

The source, sink step, equation (113), is explicit and involves no changes in cell volumes. When the source, sink term represents horizontal turbulent diffusion, it is evaluated at time level n-1, for stability (Fletcher, 1988). The advection step, equation (114), is explicit and involves changes in cell volumes. The vertical diffusion step, equation (115), which involves no changes in cell volumes, is fully implicit and unconditionally stable (Fletcher, 1988).

Rearranging equation (115), the vertical diffusion step, gives:

$$-\frac{2\theta}{\Delta_k\Delta_{k,k-1}}\left(\frac{A_b}{H}\right)_{k-1}^{n} S_{k-1}^{n+1} + \left(\frac{2\theta}{\Delta_k\Delta_{k,k-1}}\left(\frac{A_b}{H}\right)_{k-1}^{n} + H^{n+1} + \frac{2\theta}{\Delta_k\Delta_{k+1,k}}\left(\frac{A_b}{H}\right)_{k}^{n}\right)S_k^{n+1}$$
$$-\frac{2\theta}{\Delta_k\Delta_{k+1,k}}\left(\frac{A_b}{H}\right)_{k}^{n} S_{k+1}^{n+1} = H^{n+1}S_k^{**} \tag{116}$$

For salinity, temperature, and suspended sediment concentration, the generic variable S is defined vertically at cell layer centers, and the diffusivity is defined at cell layer interfaces. Equation (116) then represents a system of K equations and the boundary conditions are generally of the specified flux type. Specified surface and bottom flux boundary conditions are most conveniently incorporated in the surface and bottom cell layer source and sink terms allowing A_b at the bottom boundary, k = 0, and the surface boundary, k = K+1, to be set to zero making equation (116) tridiagonal. For turbulence intensity and turbulence length scale, equations (13,14), the generic variable S is defined vertically at cell layer interfaces and the diffusivity is defined at cell layer centers. Equation (116) then represents a system of K-1 equations for the variables at internal

interfaces with the variable values at the free surface and bottom being provided as boundary conditions. For the turbulence intensity and length scale, the boundary conditions are:

$$q_0^2 = B_1^{2/3}|\tau_0|$$
$$q_K^2 = B_1^{2/3}|\tau_K|$$
$$l_0 = 0$$
$$l_K = 0$$

where τ_0 and τ_K are the bottom and surface stress vectors respectively. Insertion of these boundary conditions results in equation (116) representing tridiagonal systems of K-1 equations for the turbulence intensity and length scale.

Without loss of generality, the notation used in analyzing the three time level advection step, equation (114), is simplified by replacing the double and single asterisk intermediate time level indicators by n+1 and n-1, respectively to give:

$$(mHS_k)^{n+1} = (mHS_k)^{n-1} - 2\theta\big(U_k(x+0.5)S_k(x+0.5) - U_k(x-0.5)S_k(x-0.5)$$
$$+V_k(y+0.5)S_k(y+0.5) - V_k(y-0.5)S_k(y-0.5) + \Delta_k^{-1}\big((WS)_k - (WS)_{k-1}\big)\big) \qquad (117)$$

where the horizontal central difference operators have been expanded about the cell volume centroid (x,y), according to equations (46,47). The cell face fluxes can be represented consistent with centered in time and space differencing as was illustrated by equations (48,49,97) or forward in time and backward or upwind in space as was illustrated by equations (50,98) for the x momentum fluxes. For the centered in time and space form, equation (117) becomes:

$$(mHS_k)^{n+1} = (mHS_k)^{n-1} - \theta\big(\tilde{U}_k(x+0.5)\big(S_k(x+1)+S_k(x)\big) - \tilde{U}_k(x-0.5)\big(S_k(x)+S_k(x-1)\big)$$
$$+\tilde{V}_k(y+0.5)\big(S_k(y+1)+S_k(y)\big) - \tilde{V}_k(y-0.5)\big(S_k(y)+S_k(y-1)\big)$$
$$+\Delta_k^{-1}\tilde{W}_k\big(S_{k+1}+S_k\big) - \Delta_k^{-1}\tilde{W}_{k-1}\big(S_k+S_{k-1}\big)\big) \qquad (118)$$

The transports in equation (118) are evaluated at the centered time level when used in the external and internal momentum equations, and are averaged to the centered time level using

$$\tilde{U}_k = 0.5\left(U_k^{n+1} + U_k^{n-1}\right) \tag{119}$$

when used in the transport equations for scalar variables.

To investigate the stability and accuracy of the centered in time and space scheme, the Fourier representation:

$$S_k = S_o \exp\left(i\omega n\theta + ik_x m_x x + ik_y m_y x + ik_z H\Delta z\right) \tag{120}$$

is introduced into equation (118) giving the characteristic polynomial

$$\lambda^2 + 2i\psi\lambda - 1 = 0 \tag{121}$$

$$\psi = \frac{u\theta}{m_x}\sin(k_x m_x) + \frac{v\theta}{m_x}\sin(k_y m_y) + \frac{w\theta}{H\Delta}\sin(k_z H\Delta) \tag{122}$$

for a steady and spatially uniform velocity field. The roots of equation (121) are:

$$\lambda = \left(\sqrt{1-\psi^2} - i\psi\right), -\left(\sqrt{1-\psi^2} + i\psi\right) \tag{123}$$

and the scheme is neutrally stable if the absolute value of ψ is less than or equal to one. The most restrictive stability condition is then

$$\frac{|u|\theta}{m_x} + \frac{|v|\theta}{m_x} + \frac{|w|\theta}{H\Delta} \le 1 \tag{124}$$

which requires the sum of the directional Courant Numbers to be less than or equal to unity. Since the centered in time and space scheme is neutrally stable when equation (124) is satisfied, the numerical scheme, like the continuous equations, has no dissipation.

Since the scheme involves three time levels, a spurious solution mode corresponding the second eigenvalue in equation (123) is introduced. Using equations (69,122,123), the dispersion relation for the physical mode of the numerical scheme is:

$$\sin(\omega\theta) = -\frac{u\theta}{m_x}\sin(k_x m_x) - \frac{v\theta}{m_x}\sin(k_y m_y) - \frac{w\theta}{H\Delta}\sin(k_z H\Delta) \quad . \tag{125}$$

The dispersion relation for the equivalent continuous equation is:

$$\omega\theta = -\frac{u\theta}{m_x}(k_x m_x) - \frac{v\theta}{m_x}(k_y m_y) - \frac{w\theta}{H\Delta}(k_z H\Delta) \quad . \tag{126}$$

Comparison of the dispersion relations shows that errors in the phase and propagation speed of the centered in time and space numerical scheme are smallest for directional Courant numbers near unity in magnitude and for small values of the wave number component, grid spacing products (Fletcher, 1988). Figure 9 shows equations (125,126) for a two-dimensional flow with directional Courant Numbers of 0.5. Although the centered in time and space scheme is desirable because it has no dissipation, its phase errors at high wave numbers are undesirable. For the transport of the horizontal momentum components in regions having large velocity gradients due to topographic variations, the centered in time and space scheme generates high wave number spatial oscillations which can corrupt the solution for the velocity field, (Smith and Cheng, 1987). The addition of horizontal diffusion to smooth the local oscillations can result in unrealistic damping of the surface wave propagation in other regions of the solution domain. When used for the transport of positive scalar fields, particularly in regions having high gradients or frontal discontinuities, the dispersive character of the centered in time and space scheme at high wave numbers is undesirable since it can lead to high wave number oscillations and unrealistic negative values of strictly positive scalar field variables.

Forward in time and backward or upwind in space representation of advective transport provides an alternative to the centered in time and space representation. The forward in time and backward or upwind in space form of equation (117) is:

$$
\begin{aligned}
&(mHS_k)^{n+1} = (mHS_k)^{n-1} \\
&-\theta\Big(\big(\tilde{U}_k(x+0.5)+\big|\tilde{U}_k(x+0.5)\big|\big)S_k^{n-1}(x)+\big(\tilde{U}_k(x+0.5)-\big|\tilde{U}_k(x+0.5)\big|\big)S_k^{n-1}(x+1) \\
&-\big(\tilde{U}_k(x-0.5)+\big|\tilde{U}_k(x-0.5)\big|\big)S_k^{n-1}(x-1)-\big(\tilde{U}_k(x-0.5)-\big|\tilde{U}_k(x-0.5)\big|\big)S_k^{n-1}(x) \\
&+\big(\tilde{V}_k(y+0.5)+\big|\tilde{V}_k(y+0.5)\big|\big)S_k^{n-1}(y)+\big(\tilde{V}_k(y+0.5)-\big|\tilde{V}_k(y+0.5)\big|\big)S_k^{n-1}(y+1) \\
&-\big(\tilde{V}_k(y-0.5)+\big|\tilde{V}_k(y-0.5)\big|\big)S_k^{n-1}(y-1)+\big(\tilde{V}_k(y-0.5)-\big|\tilde{V}_k(y-0.5)\big|\big)S_k^{n-1}(y) \\
&+\Delta_k^{-1}\Big(\big(\tilde{W}_k+\big|\tilde{W}_k\big|\big)S_k^{n-1}+\big(\tilde{W}_k-\big|\tilde{W}_k\big|\big)S_{k+1}^{n-1}-\big(\tilde{W}_{k-1}+\big|\tilde{W}_{k-1}\big|\big)S_{k-1}^{n-1}-\big(\tilde{W}_{k-1}-\big|\tilde{W}_{k-1}\big|\big)S_k^{n-1}\Big)
\end{aligned}
\qquad (127)
$$

The transports in equation (127) are evaluated at the centered time level when used in the external and internal momentum equations, and are averaged to the centered time level as illustrated by equation (119), when used in the transport equations for scalar variables. A Fourier analysis of equation (127) for a steady and spatially uniform velocity field gives the amplification factors or

eigenvalues:

$$\lambda = \pm\sqrt{1-\alpha-i\beta} \qquad (128)$$

$$\alpha = \frac{|u|(2\theta)}{m_x}\big(1-\cos(k_x m_x)\big)+\frac{|v|(2\theta)}{m_y}\big(1-\cos(k_y m_y)\big)+\frac{|w|(2\theta)}{H\Delta}\big(1-\cos(k_z H\Delta)\big) \qquad (129)$$

$$\beta = \frac{u(2\theta)}{m_x}\sin(k_x m_x)+\frac{v(2\theta)}{m_y}\sin(k_y m_y)+\frac{w(2\theta)}{H\Delta}\sin(k_z H\Delta) \qquad (130)$$

The stability of the scheme is determined by noting that the absolute

value of λ,

$$|\lambda| = \left((1-\alpha)^2 + \beta^2\right)^{\frac{1}{4}} \tag{131}$$

is maximum with respect to the three wave numbers when,

$$1-\alpha = \frac{|u|(2\theta)}{m_x}\cos(k_x m_x) + \frac{|v|(2\theta)}{m_y}\cos(k_y m_y) + \frac{|w|(2\theta)}{H\Delta}\cos(k_z H\Delta)$$

Requiring consistency with the one-dimensional results allows it to be shown that the maximum absolute value of λ is equal to the fourth root of the maximum value with respect to the wave numbers of 1-α . Thus the most restrictive stability requirement for the absolute value of λ being less than or equal to one is:

$$\frac{|u|(2\theta)}{m_x} + \frac{|v|(2\theta)}{m_y} + \frac{|w|(2\theta)}{H\Delta} \le 1 \tag{132}$$

which was previously given by Smolarkiewicz (1984). Smolarkiewicz also showed that when the stability condition is satisfied, the upwind scheme is positive definite and the sign of strictly positive scalar variables is preserved.

It is noted that when the stability condition, equation (132), is satisfied, the amplification factor or absolute value of λ will in general be less than one and the scheme is dissipative. Figure 10 shows the absolute value of the amplification factor, equation (131), for two two-dimensional flows with directional Courant Numbers of 0.5 and 0.25. For the case of the directional Courant Numbers equal to 0.5, there is no dissipation of disturbances propagating diagonal to the grid, while dissipation otherwise increases as either wave number increases or the direction of propagation changes from the diagonal. For the lower Courant Number case, dissipation increased with increasing wave number magnitude. The dissipation of high wave number or short wave length disturbances is desirable for controlling noise in the

solution, but is undesirable when high wave number features such as strong vertical stratification or horizontal frontal discontinuities are important dynamical features sought in the solution. The dispersion relation for the forward in time and upwind in space scheme is:

$$\sqrt{(1-\alpha)^2+\beta^2}\sin(2\omega\theta) = -\frac{u(2\theta)}{m_x}\sin(k_x m_x) - \frac{v(2\theta)}{m_y}\sin(k_y m_y) - \frac{w(2\theta)}{H\Delta}\sin(k_z H\Delta) \tag{133}$$

Figure 9 shows the dispersion relations for the continuous advection equation, equation (126), the centered in time and space scheme, equation (125) and the forward in time and upwind in space scheme, equation (133), for a two-dimensional flow with directional Courant Numbers of 0.5. For high wave number disturbances propagating along either grid direction the upwind scheme, although inaccurate relative to the continuous equations, is more accurate than the centered in time and space scheme.

The ideal advective transport scheme for scalar variables in environmental flows would retain the positive definite character of the forward in time and upwind in space scheme but control the dissipation of the scheme. The search for an ideal advective transport scheme has resulted in the development of numerous high order upwind schemes, modified centered in space schemes, and combined schemes as evidenced in the review by Rood (1986). Many of these schemes, although successful, are difficult to apply near boundaries in multi-dimensional flow fields. A high order upwind scheme developed by Smolarkiewicz (Smolarkiewicz, 1984, Smolarkiewicz and Clark, 1986, and Smolarkiewicz and Grabowski, 1990) and referred to as the multi-dimensional positive definite advective transport algorithm is particularly attractive because it is simple to apply near boundaries and has a sound and transparent theoretical basis. Since this scheme is used for scalar advective transport in the environmental fluid dynamics computer code, an outline of the scheme is presented here for completeness.

The central concept in the development of the Smolarkiewicz or MPDATA scheme is the determination of the sources of dissipation or damping in the forward in time and upwind in space scheme and the modification of the scheme to compensate or eliminate a significant portion of the dissipation. The sources of dissipation are identified by a consistency analysis of equation (127) which involves the use of Taylor series to determine the actual continuous equation represented by the finite difference equation. The resulting continuous equation, to second order in time and space, is:

$$\partial_t(m_x m_y hS)+\partial_x(m_y HuS)+\partial_y(m_x HvS)+\partial_z(m_x m_y wS)$$
$$=\partial_x\left(m_y H\left(\frac{m_x|u|}{2}\left(1-\frac{|u|(2\theta)}{m_x}\right)\frac{1}{m_x}\partial_x S-\frac{u(2\theta)v}{2}\frac{1}{m_y}\partial_y S-\frac{u(2\theta)w}{2}\frac{1}{H}\partial_z S\right)\right)$$
$$+\partial_y\left(m_x H\left(-\frac{v(2\theta)u}{2}\frac{1}{m_x}\partial_x S+\frac{m_y|v|}{2}\left(1-\frac{|v|(2\theta)}{m_y}\right)\frac{1}{m_y}\partial_y S-\frac{v(2\theta)w}{2}\frac{1}{H}\partial_z S\right)\right)$$
$$+\partial_z\left(m_x m_y\left(-\frac{w(2\theta)u}{2}\frac{1}{m_x}\partial_x S-\frac{w(2\theta)v}{2}\frac{1}{m_y}\partial_y S+\frac{H\Delta|w|}{2}\left(1-\frac{|w|(2\theta)}{H\Delta}\right)\frac{1}{H}\partial_z S\right)\right) \qquad (134)$$

The appearance of the second order diffusion terms in equation (134), which are the source of dissipation or damping, indicates that the scheme is only first order accurate in space. The centering of the advective field at time level n or as an average between time levels n-1 and n+1 in equation (127) eliminates a second order in time truncation term that would otherwise appear in equation (134), (Smolarkiewicz and Clark, 1986). Thus the scheme is formally second order in time. The diffusion terms in equation (134) are generally referred to as numerical diffusion and are represented by

a symmetric diffusion coefficient tensor,

$$\mathbf{D}=\begin{bmatrix} \frac{m_x|u|}{2}\left(1-\frac{|u|(2\theta)}{m_x}\right) & -\frac{u(2\theta)v}{2} & -\frac{u(2\theta)w}{2} \\ -\frac{v(2\theta)u}{2} & \frac{m_y|v|}{2}\left(1-\frac{|v|(2\theta)}{m_y}\right) & -\frac{v(2\theta)w}{2} \\ -\frac{w(2\theta)u}{2} & -\frac{w(2\theta)v}{2} & \frac{H\Delta|w|}{2}\left(1-\frac{|w|(2\theta)}{H\Delta}\right) \end{bmatrix} \tag{135}$$

The magnitude of the diagonal components of the tensor increase as the directional Courant Numbers decrease, while off diagonal components or cross wind diffusivities tend to increase in magnitude as the velocity vector becomes diagonal to the grid.

To compensate for the diffusion terms in equation (134), the velocity field is modified by the vector addition of an anti-diffusive velocity field,

$$\begin{aligned} \hat{u} &= \frac{1}{S}\left(\frac{m_x|u|}{2}\left(1-\frac{|u|(2\theta)}{m_x}\right)\frac{1}{m_x}\partial_x S-\frac{u(2\theta)v}{2}\frac{1}{m_y}\partial_y S-\frac{u(2\theta)w}{2}\frac{1}{H}\partial_z S\right) \\ \hat{v} &= \frac{1}{S}\left(-\frac{v(2\theta)u}{2}\frac{1}{m_x}\partial_x S+\frac{m_y|v|}{2}\left(1-\frac{|v|(2\theta)}{m_y}\right)\frac{1}{m_y}\partial_y S-\frac{v(2\theta)w}{2}\frac{1}{H}\partial_z S\right) \\ \hat{w} &= \frac{1}{S}\left(-\frac{w(2\theta)u}{2}\frac{1}{m_x}\partial_x S-\frac{w(2\theta)v}{2}\frac{1}{m_y}\partial_y S+\frac{H\Delta|w|}{2}\left(1-\frac{|w|(2\theta)}{H\Delta}\right)\frac{1}{H}\partial_z S\right) \end{aligned} \tag{136}$$

which in principle exactly cancels the diffusion terms in equation (134). As implemented in the MPDATA scheme, the anti-diffusive velocity field is introduced in a fractional step process. The first step involves calculating a low order solution for S at time level n+1 using equation (127) and the actual velocity field. Using the actual velocity field and the low order solution at time level n+1, the anti-diffusive velocity field is calculated using equation (136). A corrected or high order solution for S at time level n+1 is then calculated using

equation (127) in the form:

$$
\begin{aligned}
&(mHS_k)^{n+1,H} = (mHS_k)^{n+1,L} \\
&-\theta\Big(\big(\hat{U}_k(x+0.5)+\big|\hat{U}_k(x+0.5)\big|\big)S_k^{n+1,L}(x)+\big(\hat{U}_k(x+0.5)-\big|\hat{U}_k(x+0.5)\big|\big)S_k^{n+1,L}(x+1) \\
&-\big(\hat{U}_k(x-0.5)+\big|\hat{U}_k(x-0.5)\big|\big)S_k^{n+1,L}(x-1)-\big(\hat{U}_k(x-0.5)-\big|\hat{U}_k(x-0.5)\big|\big)S_k^{n+1,L}(x) \\
&+\big(\hat{V}_k(y+0.5)+\big|\hat{V}_k(y+0.5)\big|\big)S_k^{n+1,L}(y)+\big(\hat{V}_k(y+0.5)-\big|\hat{V}_k(y+0.5)\big|\big)S_k^{n+1,L}(y+1) \\
&-\big(\hat{V}_k(y-0.5)+\big|\hat{V}_k(y-0.5)\big|\big)S_k^{n+1,L}(y-1)+\big(\hat{V}_k(y-0.5)-\big|\hat{V}_k(y-0.5)\big|\big)S_k^{n+1,L}(y) \\
&+\Delta_k^{-1}\Big(\big(\hat{W}_k+\big|\hat{W}_k\big|\big)S_k^{n+1,L}+\big(\hat{W}_k-\big|\hat{W}_k\big|\big)S_{k+1}^{n+1,L}-\big(\hat{W}_{k-1}+\big|\hat{W}_{k-1}\big|\big)S_{k-1}^{n+1,L}-\big(\hat{W}_{k-1}-\big|\hat{W}_{k-1}\big|\big)S_k^{n+1,L}\Big)
\end{aligned}
\tag{137}
$$

Since the anti-diffusive velocity field, equation (136), does not satisfy the continuity equations (45,111), the anti-diffusive velocity should be set to zero on all open boundaries such that global continuity of the transported variable is maintained. The application of equation (137) will also introduce numerical diffusion, and another anti-diffusive velocity field can be calculated and an additional application of equation (137) can be made. In principle this can continue until the numerical diffusion is insignificantly small, however computationally more than two anti-diffusive steps tends to be inefficient.

The MPDATA scheme, althought strictly sign preserving, can suffer from dispersive ripples similar to other higher order advection schemes, (Smolarkiewicz and Grabowski, 1990). The dispersive ripples can be controlled by applying the scheme in conjunction with flux corrected transport methodology (Zalesak, 1979) as described by Smolarkiewicz and Grabowski. When applied in the flux corrected transport form, the solution of equation (127) is the low order positive definite solution, while the solution of equation (137) is the high order solution. The advective fluxes in the high order solution are however multiplied by a flux limiter, which is less than unity, such that the high order solution is free of dispersive ripples. The

calculation of the flux limiter is described by Smolarkiewicz and Grabowski (1990) and Zalesak (1979).

Since the three time level fractional step scheme, equations (113-115), for the transport equations introduces a spurious computational solution mode, periodic insertion of a two time level correction step as discussed in Section 4 is necessary. The two time level fractional step scheme is given by:

$$S_k^* = S_k^n + \theta(mH^n)^{-1}(Q_S)_k^n \tag{138}$$

$$(mH)^{n+1} S_k^{**} = (mH)^n S_k^* - \theta\left(\delta_x^\zeta (U_k S_k) + \delta_y^\zeta (V_k S_k) + \Delta_k^{-1}\left((WS)_k - (WS)_{k-1}\right)\right)^{n+\frac{1}{2}} \tag{139}$$

$$(HS_k)^{n+1} - \theta\left(\left(\frac{(H^{-1}A_b)_k^{n+\frac{1}{2}}(S_{k+1} - S_k)^{n+1}}{\Delta_k \Delta_{k+1,k}}\right) - \left(\frac{(H^{-1}A_b)_{k-1}^{n+\frac{1}{2}}(S_k - S_{k-1})^{n+1}}{\Delta_k \Delta_{k,k-1}}\right)\right) = H^n S_k^{**} \tag{140}$$

The vertical diffusion fractional step, equation (140) is rearranged to give a tridiagonal system similar to equation (116). The vertical diffusivity divided by depth in equation (140) can be an arithmetic or geometric average between the value at time level n and the value at time level n+1 from the three time level step.

The advective fractional step, equation (139), is forward in time and upwind in space and is given by:

$$
\begin{aligned}
&(mHS_k)^{n+1} = (mHS_k)^n \\
&-\frac{\theta}{2}\Bigg(\left(\tilde{U}_k(x+0.5)+\left|\tilde{U}_k(x+0.5)\right|\right)^{n+\frac{1}{2}} S_k^n(x) + \left(\tilde{U}_k(x+0.5)-\left|\tilde{U}_k(x+0.5)\right|\right)^{n+\frac{1}{2}} S_k^n(x+1) \\
&-\left(\tilde{U}_k(x-0.5)+\left|\tilde{U}_k(x-0.5)\right|\right)^{n+\frac{1}{2}} S_k^n(x-1) - \left(\tilde{U}_k(x-0.5)-\left|\tilde{U}_k(x-0.5)\right|\right)^{n+\frac{1}{2}} S_k^n(x) \\
&+\left(\tilde{V}_k(y+0.5)+\left|\tilde{V}_k(y+0.5)\right|\right)^{n+\frac{1}{2}} S_k^n(y) + \left(\tilde{V}_k(y+0.5)-\left|\tilde{V}_k(y+0.5)\right|\right)^{n+\frac{1}{2}} S_k^n(y+1) \\
&-\left(\tilde{V}_k(y-0.5)+\left|\tilde{V}_k(y-0.5)\right|\right)^{n+\frac{1}{2}} S_k^n(y-1) + \left(\tilde{V}_k(y-0.5)-\left|\tilde{V}_k(y-0.5)\right|\right)^{n+\frac{1}{2}} S_k^n(y) \\
&+\Delta_k^{-1}\Bigg(\left(\tilde{W}_k+\left|\tilde{W}_k\right|\right)^{n+\frac{1}{2}} S_k^n + \left(\tilde{W}_k-\left|\tilde{W}_k\right|\right)^{n+\frac{1}{2}} S_{k+1}^n - \left(\tilde{W}_{k-1}+\left|\tilde{W}_{k-1}\right|\right)^{n+\frac{1}{2}} S_{k-1}^n - \left(\tilde{W}_{k-1}-\left|\tilde{W}_{k-1}\right|\right)^{n+\frac{1}{2}} S_k^n \Bigg)\Bigg)
\end{aligned}
\tag{141}
$$

where the single and double asterisks have been replaced by n and n+1. The flows in equation (141) are averages of the values at n and the values at n+1 computed from the three time level scheme. The stability condition and dispersion relation for the two time level advection scheme are given by replacing 2θ in equations (132,133) with θ. The anti-diffusive correction to equation (141) follows directly from equations (136,137) with 2θ being replaced by θ.

7. THE ENVIRONMENTAL FLUID DYNAMICS COMPUTER CODE

The computational algorithms or schemes described in Sections 3-6 for the solution of the momentum, continuity and transport equations (2-9) have been implemented in the Environmental Fluid Dynamics Computer Code using the Fortran 77 language. The code is organized into preliminary processing, computational, continuous processing and post processing sections. The preliminary processing section includes subroutines for data input, initialization, and restarting. A separate Fortran program is used for curvilinear orthogonal horizontal grid generation using the weak constraint

method of Ryskin and Leal (1983) with modifications proposed by Chikhliwala and Yortsos (1985).

The computational sections of the code sequentially solve the external mode equations, the internal mode equations, and the transport equations for salinity, temperature, turbulence intensity, and turbulence length scale. Two time level correction steps are periodically inserted at user specified intervals, usually every four to eight three time level steps. To reduce memory requirements, three dimensional variables are stored in two-dimensional arrays with the inner array index used for active water cells in the horizontal and the outer index used for the vertical cell layer. Since the number of horizontal cells will greatly exceed the number of vertical cell layers, the inner do loops over the horizontal are very long relative to the outer do loops over the vertical allowing efficient vectorization of the code.

The continuous processing section of the code includes subroutines for writing files for graphics and visualization of the transient behavior of vector and scalar variables and subroutines for inplace least squares harmonic analysis and filtering of variables at user specified locations. Two specialized subroutines can be activated to write filtered or time averaged transport files to drive long term contaminant transport and water quality simulation models. A Lagrangian trajectory subroutine allows simulation of floating and neutrally buoyant drifter and particle trajectories from specified time and space release points. Files for restarting the simulation in progress can also be written at specified intervals. The post processing section of the code produces a final restart file and various graphics and visualization files for mean or averaged variables.

The code is designed to be an engineering tool for environmental impact assessment and management and a scientific tool to investigate environmental flow dynamics in real and hypothetical situations. When the code is used as an engineering or scientific tool

applied to model a prototype flow, a calibration and verification process is essential. The calibration of the code to a prototype situation involves adjustment of boundary conditions and forcing functions and boundary roughness, equation (109), such that the model reasonably reproduces a known response. For estuarine and coastal ocean flows, the known response would include time series of field measurements of free surface displacement, horizontal velocity magnitude and direction, salinity and temperature. The calibrated model is then verified by simulating or predicting an entirely different response. The inplace filtering and least squares harmonic analysis features of the code are particularly useful in extracting information for comparsion with field measurements in the calibration and verification processes. After calibration and verification, the code or model can be used to simulate the impacts of engineering projects or extreme hydrologic conditions for example, or to investigate basic flow processes.

8. SUMMARY

The theoretical and computational aspects of a three-dimensional computer code for environmental fluid flow simulation have been presented. The code is applicable to a wide range of environmenatal flows which are vertically hydrostatic and of the boundary layer type. The computer code solves the vertically hydrostatic, free surface, variable density, turbulent-averaged equations of motion and transport equations for turbulence intensity and length scale, salinity and temperature in a stretched,vertical coordinate system, and horizontal coordinate systems which may be Cartesian or curvilinear-orthogonal. Equations describing the transport of suspended sediment and dynamically neutral conservative and nonconservative tracers are also solved. The code uses a three time level, finite difference scheme with a internal-external mode splitting procedure to separate the internal shear or baroclinic mode from the external free surface gravity wave or barotropic mode. The external mode solution is implicit, and simultaneously computes the

two-dimensional surface elevation field by a multicolor SOR procedure. The external solution is completed by the calculation of the depth integrated barotropic velocities using the new surface elevation field. The implicit external solution allows large time steps which are constrained only by the stability criteria of the explicit advection scheme used for the nonlinear accelerations. The internal solution, at the same time step as the external, is implicit with respect to vertical diffusion. The internal solution of the momentum equations is in terms of the velocity shear, which results in the simplest and most accurate form of the baroclinic pressure gradients and eliminates the over determined character of alternate internal mode formulations. The vertical diffusion coefficients for momentum, mass and temperature are determined by the second moment closure scheme of Mellor and Yamada, (Mellor and Yamada, 1982, Blumberg and Mellor, 1987, and Galperin *et al*, 1988) which involves the use of analytically determined stability functions and the solution of transport equations for the turbulence intensity and length scale. Time splitting inherent in the three time level scheme is controlled by periodic insertion of a two time level step. The code include various options for advective transport, including the centered in time and space scheme, the forward in time and upwind in space scheme, and Smolarkiewicz's multidimensional positive definite advective transport algorithm, (Smolarkiewicz and Clark, 1986, Smolarkiewicz and Grabowski, 1990), which is used in the scalar transport equations. The code is written in standard Fortran 77, and is designed to economize mass storage by storing only active water cell variables in memory. Particular attention has also been given to minimizing logical operations, and the code is highly vectorizable. The code was originally developed on a DEC VAX computer and has been ported to Sun workstations, Macintosh and 386 PC's, and Cray and Convex supercomputers.

REFERENCES

Arakawa, A., and V. R. Lamb, 1977: Computational design of the basic dynamical processes of the UCLA general circulation model. *Methods in Computational Physics, Vol 17,* Academic Press, 174-265.

Blumberg, A. F., and G. L. Mellor, 1987: A description of a three-dimensional coastal ocean circulation model. *Three-dimensional coastal ocean models,* Editor: N. S. Heaps, American Geophysical Union, 1-16.

Bryan, K., 1969: A numerical method for the study of the circulation of the world ocean. *J. Comp. Phys.*, **4**, 347-376.

Chikhliwala, E. D., and Y. C. Yortsos, 1985: Application of orthogonal mapping to some two-dimensional domains. *J. Comp. Phys.*, **57**, 391-402.

Chang, J., (Ed.) 1977: *Methods in computational physics, Vol. 17,* Academic Press.

Clark, T. L., 1977: A small-scale dynamics model using a terrain-following coordinate transformation. *J. Comp. Phys.*, **24**, 186-215.

Clark, T. L., and W. D. Hall, 1991: Multi-domain simulations of the time dependent Navier-Stokes equations: benchmark error analysis of some nesting procedures. *J. Comp. Phys.*, **92**, 456-481.

Fischer, H. B., *et al*, 1979: *Mixing in inland and coastal waters,* Academic Press, 483 pp.

Fletcher, C. J. A., 1988: *Computational techniques for fluid dynamics 1 & 2,* Springer-Verlag, 409 & 484 pp.

Foreman, M. G. G., 1983: An analysis of two-step time discretizations in the solution of the linearized shallow water equations. *J. Comp. Phys.*, **51**, 454-483.

Galperin, B., L. H. Kantha, S. Hassid, and A. Rosati, 1988: A quasi-equilibrium turbulent energy model for geophysical flows. *J. Atmos. Sci.*, **45**, 55-62.

Hageman, L. A., and D. M. Young, 1981: *Applied iterative methods*, Academic Press, 386pp.

Haltiner, G. J., and R. T. Williams, 1980: *Numerical prediction and dynamic meteorology*, Wiley, 477 pp.

Hamrick, J. M., 1986: Long-term dispersion in unsteady skewed free surface flow. *Estuar. Coast. Shelf Sci.*, **23**, 807-845.

Heaps, N. S., Editor, 1987: *Three-dimensional coastal ocean models*, America Geophysical Union, 208 pp.

Liu, S. K., and J. J. Leendertse, 1975: Multidimensional numerical modeling of estuaries and coastal sea. *Advances in Hydroscience, Vol. 10*, Editor: V. T. Chow, Academic Press, 95-164.

Madala, R. V., and S. A. Piacsek, 1977: A semi-implicit numerical model for baroclinic oceans. *J. Comp. Phys.*, **23**, 167-178.

Mellor, G. L., 1991: An equation of state for numerical models of oceans and estuaries. *J. Atmos. Oceanic Tech.*, **8**, 609-611.

Mellor, G. L., and A. F. Blumberg, 1985: Modeling vertical and horizontal diffusivities with the sigma coordinate system. *Mon. Wea. Rev.*, **20**, 851-875.

Mellor, G. L., and T. Yamada, 1982: Development of a turbulence closure model for geophysical fluid problems. *Rev. Geophys. Space Phys.*, **20**, 851-875.

Nihoul, J. C. J., and B. M. Jamart, Editors, 1987: *Three-dimensional models of marine and estuarine dynamics*, Elsevier, 629 pp.

Peyret, R., and T. D. Taylor, 1983: *Computational methods for fluid flow*, Springer-Verlag, 358 pp.

Pielke, R. A., 1984: *Mesoscale Meteorological Modeling*, Academic Press, 612 pp.

Press, W. H., B. P. Flannery, S. A. Teukolsky and W. T. Vetterling, 1986: *Numerical recipes, the art of scientific computing*, Cambridge University Press, 818 pp.

Rood, R. B., 1986: Numerical advection algorithms and their role in atmospheric transport and chemistry. *Rev. Geophys. Phys.*, **25**, 71-100.

Ryskin, G., and L. G. Leal, 1983: Orthogonal mapping. *J. Comp. Phys.*, **50**, 71-100.

Semtner, A. J., 1974: An oceanic general circulation model with bottom topography. Dept. of Meteorology, Univ. Calif., Los Angeles, *Tech. Rept. 9*, 41 pp.

Simons, T. J., 1973: Development of three-dimensional numerical models of the Great Lakes. Canada Centre for Inland Waters, *Scientific Series 12*, 26 pp.

Simons, T. J., 1974: Verification of numerical models of Lake Ontario, Part 1. Circulation in spring early summer. *J. Phys. Oceanogr.*, **4**, 507-523.

Smagorinsky, J., 1963: General circulation experiments with the primative equations, I. The basic experiment. *Mon. Weather Rev.*, **91**, 99-164.

Smith,L. H., and R. T. Cheng, 1987: Tidal and tidally averaged circulation characteristics of Suisun Bay, California. *Water Resour. Res.*, **23**, 143-155.

Smolarkiewicz, P. K., 1984: A fully multidimensional positive definite advection transport algorithm with small implicit diffusion. *J. Comp. Phys.*, **54**, 325-362.

Smolarkiewicz, P. K., and T. L. Clark, 1986: The multidimensional positive definite advection transport algorithm: further development and applications. *J. Comp. Phys.*, **67**, 396-438.

Smolarkiewicz, P. K., and W. W. Grabowski, 1990: The multidimensional positive definite advection transport algorithm: nonoscillatory option. *J. Comp. Phys.*, **86**, 355-375.

Vinokur, M., 1974: Conservation equations of gas dynamics in curvilinear coordinate systems. *J. Comp. Phys.*, **50**, 71-100.

Zalesak, S. T. , 1979: Fully multidimensional flux-corrected transport algorithms for fluids. *J. Comp. Phys.*, **31**, 335-362.

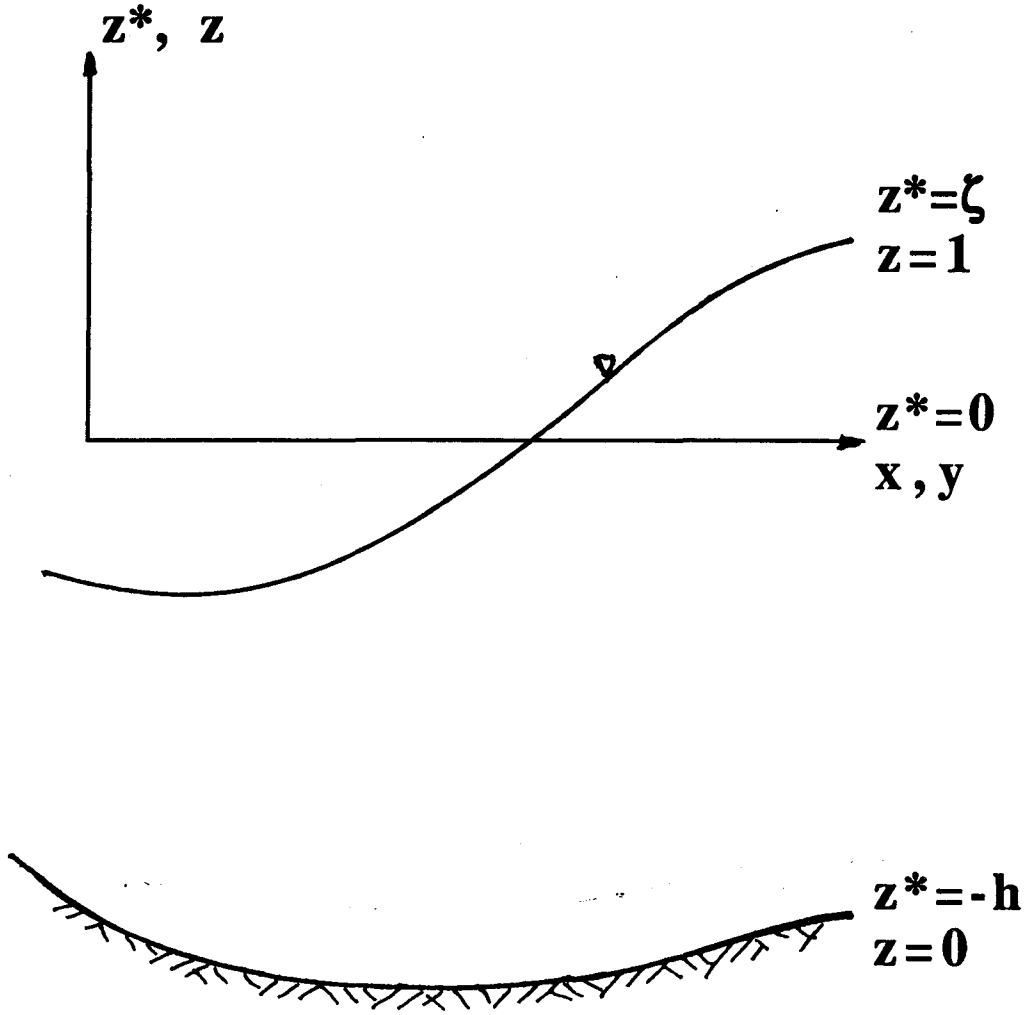

Figure 1. The stretched vertical coordinate system

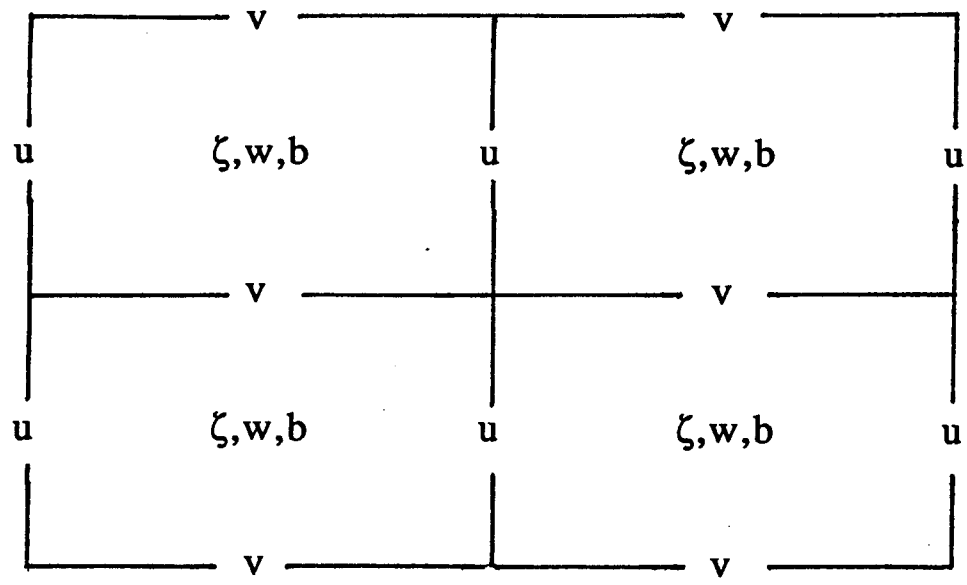

Figure 2. Free surface displacement centered horizontal grid.

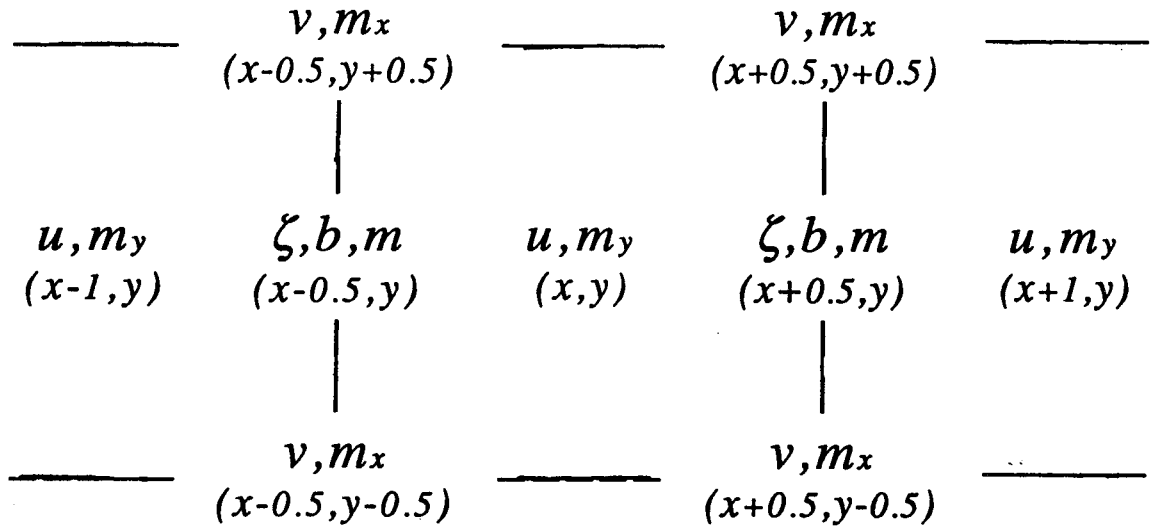

Figure 3. U centered grid in the horizontal (x,y) plane.

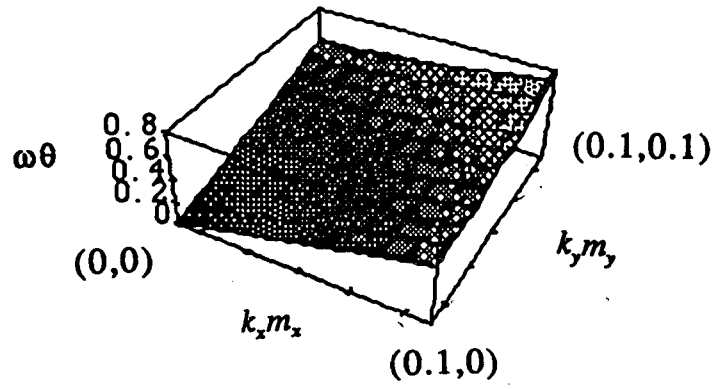

(a) Continuous equations

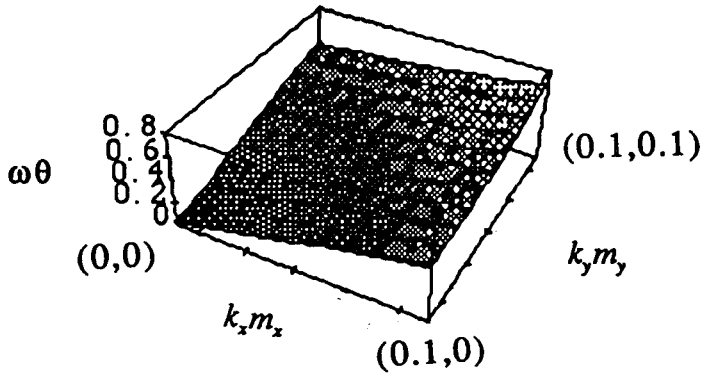

(b) Two time level trapezoidal difference equations

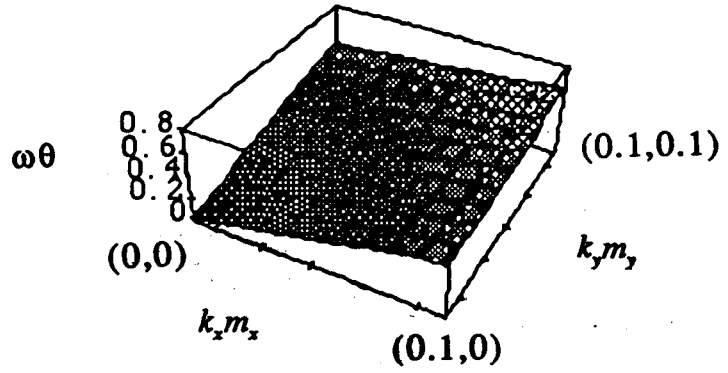

(c) Three time level leap-frog trapezoidal difference equations

Figure 4. Dispersion relations: $\omega\theta$, vertical axis, versus $k_x m_x$ and $k_y m_y$, horizontal axes, for wave propagation schemes.

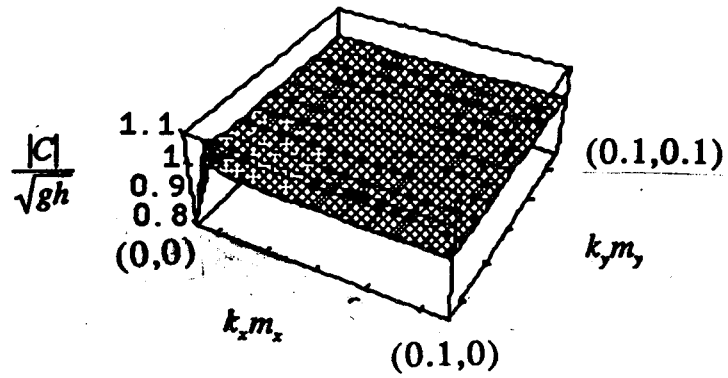

(a) Continuous Equations

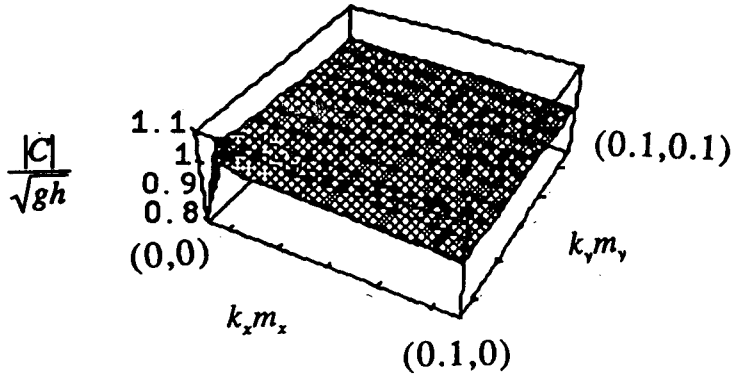

(b) Two time level trapezoidal difference equations

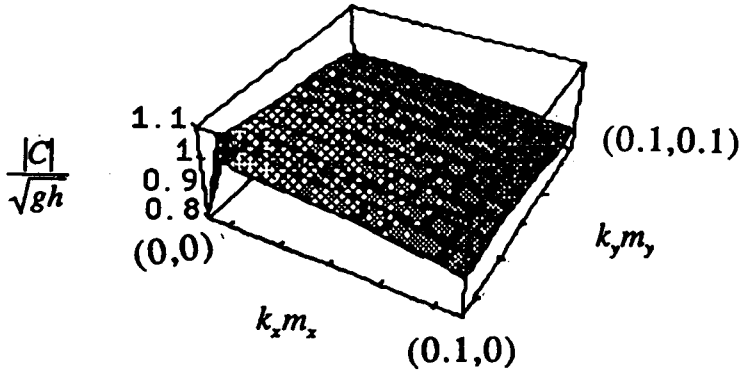

(c) Three time level leap-frog trapezoidal difference equations

Figure 5. Magnitude of phase velocity, |c|/sqrt(gh), vertical axis, as a function of horizontal wave number, kxmx and kymy, horizontal axes.

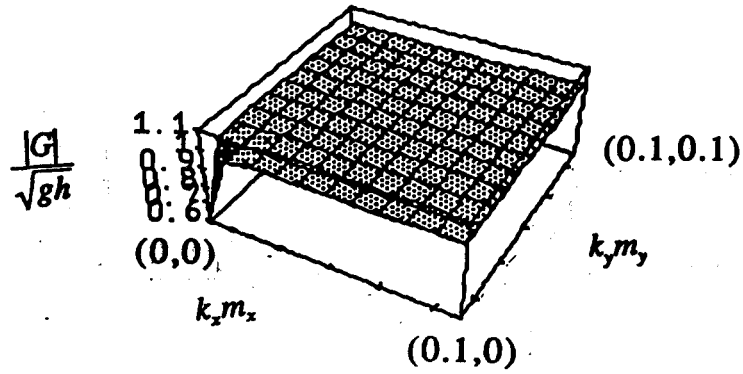

(a) Continuous Equations

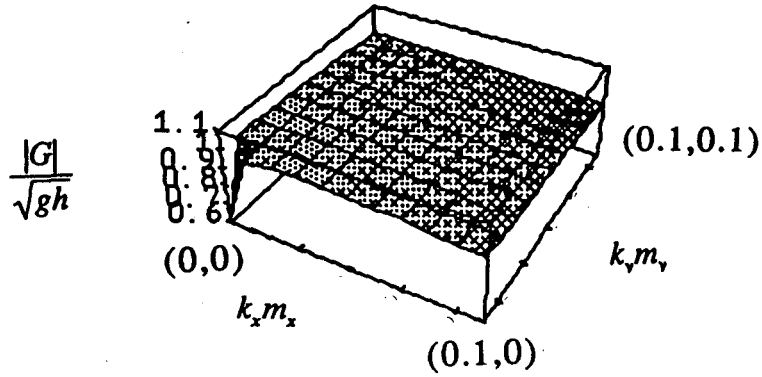

(b) Two time level trapezoidal difference equations

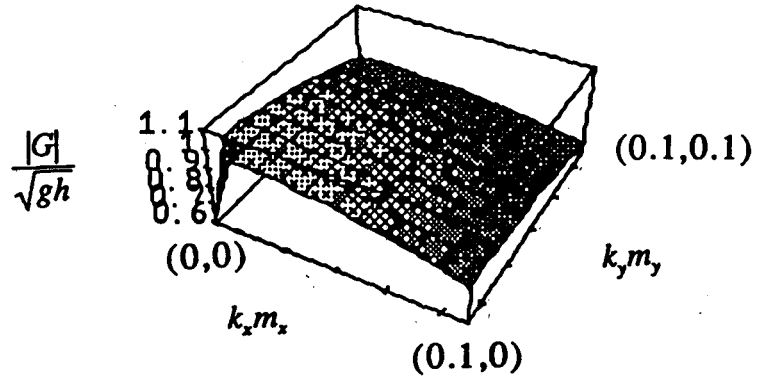

(c) Three time level leap-frog trapezoidal difference equations

Figure 6. Magnitude of group velocity, |G|/sqrt(gh), vertical axis, as a function of horizontal wave number, kxmx and kymy, horizontal axes.

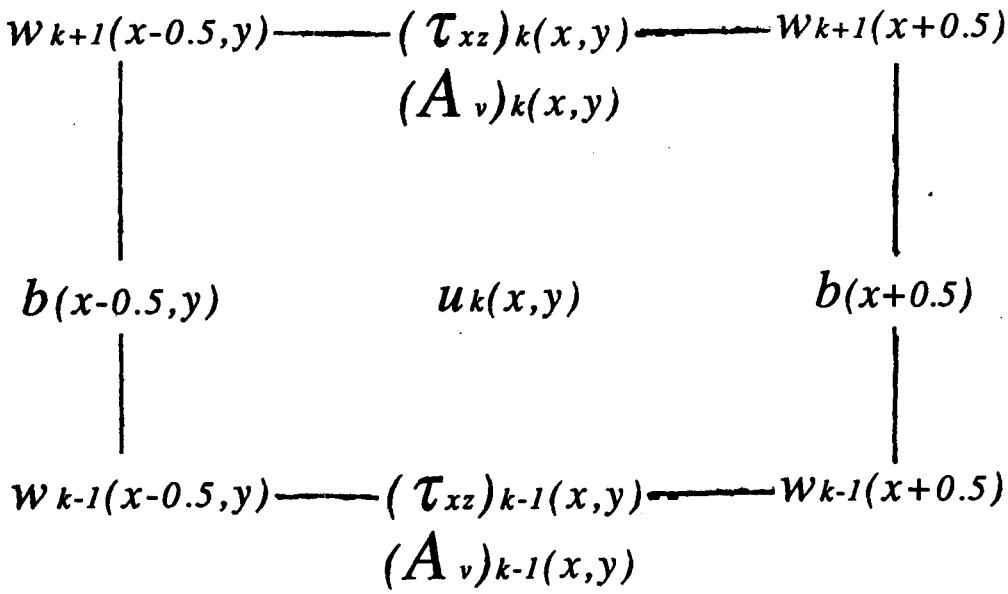

Figure 7. U centered grid in the vertical (x,z) plane.

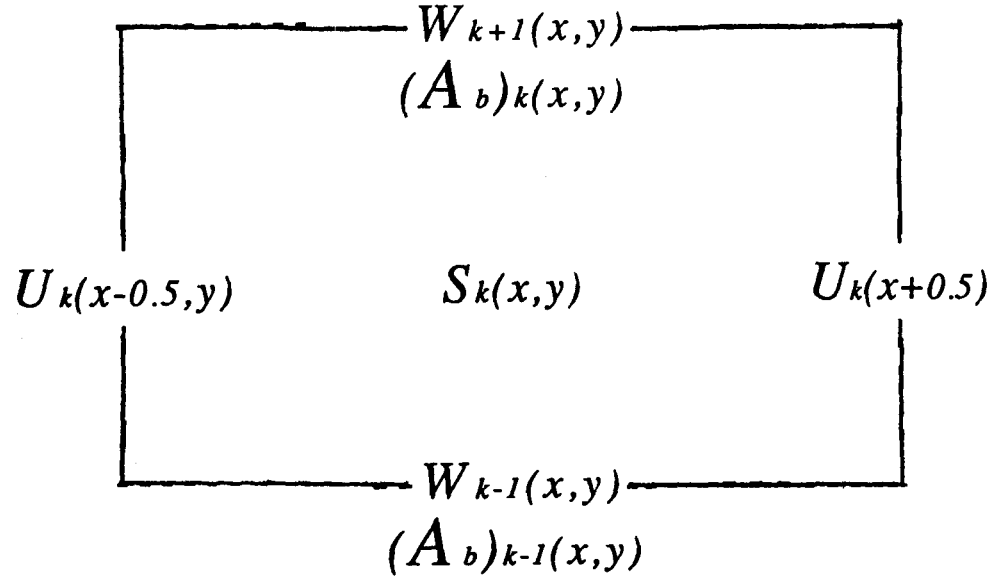

Figure 8. S centered grid in the vertical (x,z) plane.

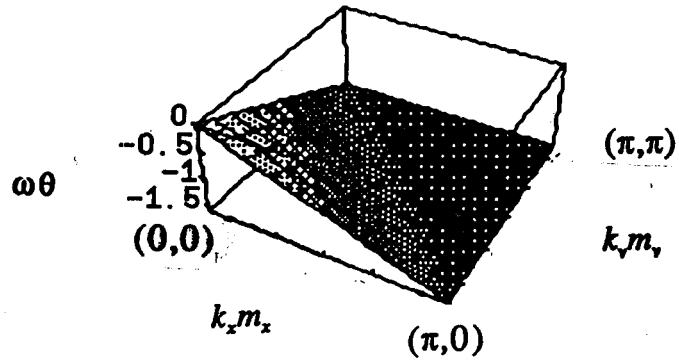

(a) Continuous equation (values less than -1.5 shown as -1.5)

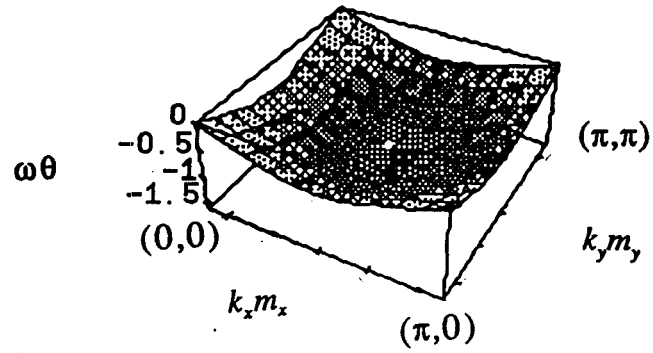

(b) Three time level centered in time and space

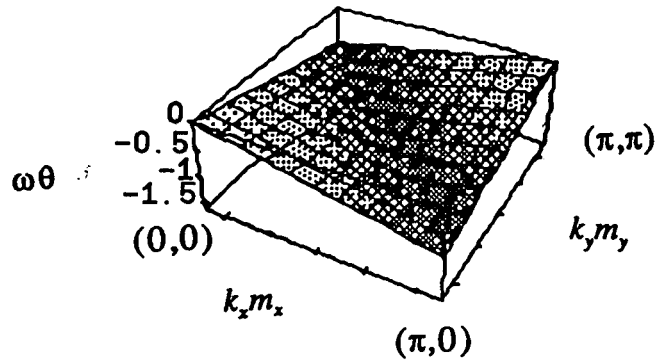

(c) Three time level forward in time and upwind in space

Figure 9. Dispersion relations: $\omega\theta$, vertical axis, versus $k_x m_x$ and $k_y m_y$, horizontal axes, for advection scheme. Courant Numbers = 0.5.

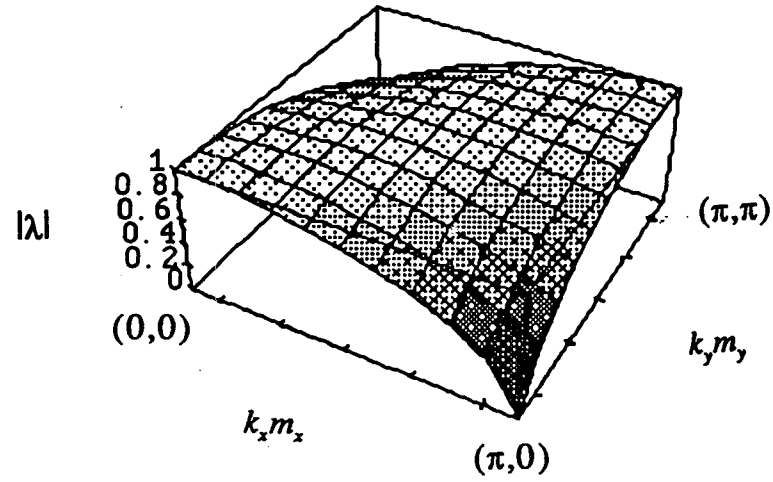

(a) Horizontal Directional Courant Numbers equal to 0.5

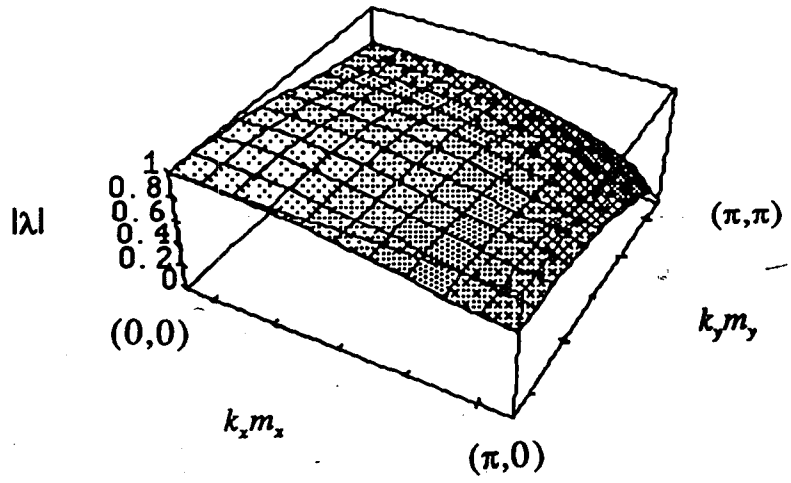

(a) Horizontal Directional Courant Numbers equal to 0.25

Figure 10. Magnitude of amplification factor, vertical axis, versus $k_x m_x$ and $k_y m_y$, horizontal axes, for upwind advection scheme